www.aem-journal.com

Oxidation-Resistant Environmental Barrier Coatings for Mo-Based Alloys: A Review

Caren Gatzen,* Iryna Smokovych, Michael Scheffler, and Manja Krüger

Molybdenum-based materials offer high melting temperatures and promising mechanical properties; therefore, they are potential candidates for high-temperature components, such as turbine blades. However, at temperatures above 700 °C, molybdenum suffers from severe pesting phenomenon, leading to decomposition of the component. Therefore, oxidation-resistant environmental barrier coatings are crucial to prevent the material from degradation and to maintain its excellent mechanical properties at high temperatures. This review provides a detailed overview on the different coating concepts for Mo and Mo-based alloys.

1. Introduction

1.1. New Materials for High-Temperature Components

High-temperature processes and applications, such as aerospace and land-based gas turbine engines, are continuously optimized to achieve maximum efficiency. The efficiency can be increased by increasing the maximum service temperature of the engine. Nowadays, nickel-based superalloys with the melting temperatures around 1350 °C are used in the hottest engine parts. ^[1] Using complex cooling systems and thermal barrier coatings (TBCs), the surface temperature of the component was increased to 1150 °C. ^[2] Nevertheless, further temperature increase is not possible as the melting temperatures of the superalloys limit the service temperature. Moreover, the complex cooling leads to a drastic loss of efficiency. Therefore, there is a need for new materials with high melting temperatures and excellent mechanical properties. ^[1,3]

New materials for turbine components should provide high melting temperatures, high tensile strength, sufficient ductility,

Dr. C. Gatzen
Institute of Energy and Climate Research
Microstructure and Properties of Materials (IEK-2)
Forschungszentrum Jülich GmbH
Jülich 52425, Germany
E-mail: caren.gatzen@rwth-aachen.de

Dr. C. Gatzen, Dr. I. Smokovych, Prof. M. Scheffler, Prof. M. Krüger Institute for Materials and Joining Technology Otto von Guericke University Magdeburg P.O. Box 4120, Magdeburg 39016, Germany

The ORCID identification number(s) for the author(s) of this article can be found under https://doi.org/10.1002/adem.202001016.

© 2020 The Authors. Advanced Engineering Materials published by Wiley-VCH GmbH. This is an open access article under the terms of the Creative Commons Attribution License, which permits use, distribution and reproduction in any medium, provided the original work is properly cited.

DOI: 10.1002/adem.202001016

and low creep rates to replace the nickel-based superalloys. Furthermore, the materials are exposed to aggressive combustion gases and need to be resistant to oxidation and corrosion. As Perepezko^[1] showed, operation at 1300 °C without complex cooling systems could increase output power by almost 50%. According to the Johnson relation, operation without cooling system and TBC requires the melting temperatures of at least 2500 °C. ^[4] A further advantage of materials with high melting temperatures is the fact that they usually have low creep

rates, which is favorable for turbine components.^[4]

There is only a limited number of ceramics, intermetallic compounds, and refractory metals, which offer the melting temperatures above 2500 °C. Brittleness is a major problem with single components made of ceramics or intermetallic phases. In contrast, refractory metals, such as molybdenum, offer sufficient ductility and high melting temperatures (2623 °C^[5]). However, an important drawback is the catastrophic oxidation behavior of Mo-rich alloys at intermediate temperatures. Therefore, this article will give an overview of the oxidation mechanisms of Mo and Mo-based alloys and the evaluation of different protective coating concepts.

1.2. Mo Pesting

In oxidizing environments, most metals form protective oxide scales on the surface, which slow down further oxidation. Molybdenum also oxidizes at elevated temperatures in the presence of oxygen. Unfortunately, this oxide layer is non-protective as MoO_3 sublimates at the temperatures around $730\,^{\circ}\text{C}$. [6] This leads to a severe weight loss and degradation of the component.

Compared with pure molybdenum, molybdenum silicides offer higher oxidation resistance, because a protective silica scale is formed on the surface; however, their melting temperatures are somewhat lower (>2000 °C^[7]). The formation of the silica scale can be enhanced by the addition of boron, leading to the formation of a protective glassy borosilicate layer on the surface. Studies showed that the addition of boron drastically influences the oxidation behavior of Mo-Si alloys. [8] The steady-state oxidation rates (20-100 h, without initial weight loss) of different Mo-Si-B alloys with varying B/Si ratio are shown in Figure 1. As shown in Figure 1, the weight loss due to volatilization of MoO₃ prevails when the B-content of the alloy is low. With increasing B-content, the weight loss due to volatilization of Mo oxides and the weight gain due to the formation of a protective oxide scale approach each other. At an atomic B/Si ratio of 0.23, weight gain and weight loss compensate each other.

15272648, 2021, 4, Downloaded from https://onlinelibrary.wiley.com/doi/10.1002/adem.202001016 by Forschungszentrum Jülich GmbH Research Center, Wiley Online Library on [01/05/2024]. See the Terms

ms) on Wiley Online Library for rules of use; OA articles are governed by the applicable Creative Commons

www.advancedsciencenews.com

www.aem-journal.com

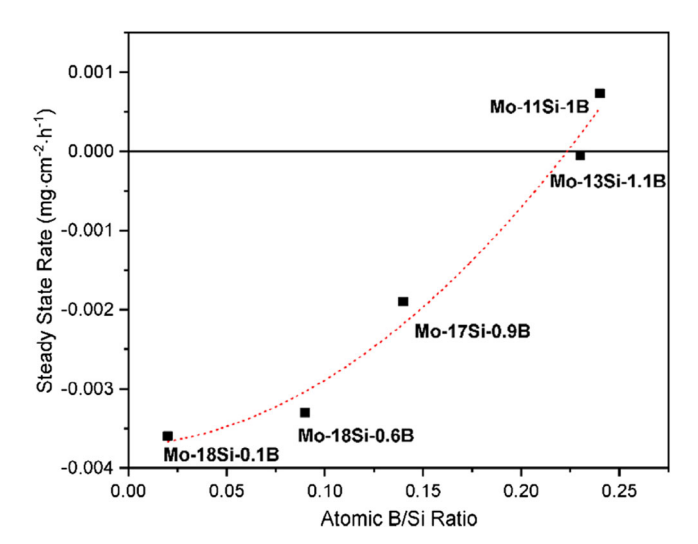


Figure 1. Measured steady-state oxidation rates of Mo–Si–B alloys with varying B/Si atomic ratio during $20-100 \, h$ oxidation test at $1000 \, ^{\circ} \text{C}$. Black squares: Data from Meyer et al. [8] Dotted line: Guideline to the eye.

Higher B-contents (0.24) lead to an overall weight gain of the sample as oxide formation prevails.

A typical Mo–Si–B alloy consists of a continuous body-centered-cubic solid-solution $\alpha\text{-Mo-phase}$, which acts as a matrix. The function of the $\alpha\text{-Mo}$ matrix can be compared with the $\gamma\text{-phase}$ in nickel-based superalloys. Phases, such as Mo₃Si (A15), Mo₅Si₃ (T1), and Mo₅SiB₂ (T2), are embedded in the Mo matrix. These phases drastically influence the properties of the alloy. Although alloying with Si and B, oxidation of the material at high temperatures is still challenging. The oxidation behavior has been studied in detail by Parthasarathy et al., and four stages of oxidation were determined, which are shown in **Figure 2**.

At low temperatures between 500 and $600\,^{\circ}$ C, a parabolic weight gain is observed. This can be explained by the simultaneous oxidation of Mo, Si, and B. Although, the formation of SiO_2 is energetically preferred, its high viscosity at this temperature prevents the formation of a continuous protective scale. Consequently, near-surface molybdenum oxidizes to MoO_3 , which can be found on the surface as well. The concurring oxidation of Mo and Si leads to a decreased oxidation rate compared with pure Mo.

At 700 ± 50 °C, MoO₃ starts to volatilize; at this stage, a linear weight loss with a rate constant of 3.3 mg cm⁻² h⁻¹ is reported.

In this temperature regime, boron is oxidized, leading to the formation of a porous borosilicate-glass scale. However, the formed scale is still not protective; on the contrary, no difference in oxidation behavior between Mo and Mo–Si–B was found. The porous scale allows oxygen to penetrate the scale and enables evaporation of MoO₃. Consequently, the reaction of Mo to MoO₃ is the rate-determining step.^[9]

With rising temperature (>800 °C), more boron is oxidized to B_2O_3 . The high boron content lowers the viscosity of the oxide scale. On the one hand, this allows the formation of a continuous oxide scale. On the other hand, the low viscosity allows the formation of bubbles and, therefore, enables the penetration of O_2 and evaporation of O_3 through the scale. In addition, boron is known to enhance the oxygen diffusivity, leading to a further increase in the oxidation rate.

Further temperature increase leads to enhanced evaporation of B_2O_3 . Consequently, the viscosity of the oxide scale increases constantly. Accordingly, the oxygen and MoO_3 permittivity of the scale decrease. The viscosity can increase by up to ten orders of magnitude; hence, the oxygen diffusivity can be reduced by six orders of magnitude. Finally This complex oxidation mechanism leads to the fact that the oxidation at $800\,^{\circ}\text{C}$ is significantly faster than at $1300\,^{\circ}\text{C}$. Mendiratta et al. He significantly reduced that oxidation at $800\,^{\circ}\text{C}$ can be significantly reduced using pre-oxidized material (1300 $^{\circ}\text{C}$). Tests revealed that $100\,\text{h}$ of pre-oxidation at reduced O_2 pressure is sufficient to suppress the pesting behavior during oxidation at $1200\,^{\circ}\text{C}$.

Mechanical properties and oxidation resistance are strongly dependent on the ratio of α -Mo, Mo₃Si, Mo₅SiB₂, and Mo₅Si₃ phases. Therefore, a lot of research is focused on the alloying of Mo–Si–B to find compositions that combine high oxidation resistance and favorable mechanical properties. [17–20] However, the desired material properties require different microstructures according to **Figure 3**.

For high oxidation resistance, silicide-rich alloys with small discontinuous grains are preferred. A coarse microstructure with only small volume fraction of α -Mo leads to high creep resistance. In contrast to this, high damage tolerance is achieved by large volume fractions of continuous α -Mo grains. These contradictory microstructures are shown in Figure 3.

The oxidation behavior of several Mo-based samples is compared in **Figure 4**. For better comparison of samples with different oxidation times, a weight loss rate (in $mg cm^{-2} h^{-1}$) was introduced by dividing the measured weight loss (in $mg cm^{-2}$) by the test duration (in h). As discussed earlier, the pesting behavior of pure Mo leads to high weight losses. Alloying of

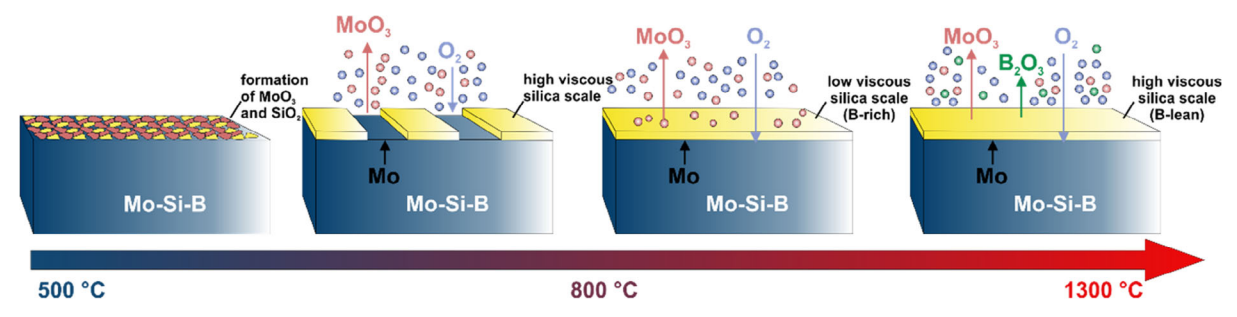


Figure 2. Schematic oxidation mechanism of Mo-Si-B alloys at elevated temperatures as described by Parthasarathy et al. [9]

15272648, 2021, 4, Downloaded from https://onlinelibrary.wiley.com/doi/10.1002/adem.202001016 by Forschungszentrum Jülich GmbH Research Center, Wiley Online Library on [0.105/2024]. See the Terms and Conditions

onditions) on Wiley Online Library for rules of use; OA articles are governed by the applicable Creative Commons

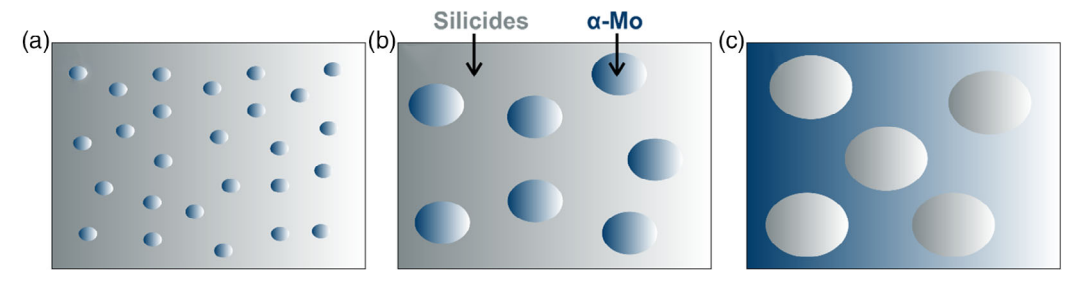


Figure 3. Schematic illustrations of optimized Mo–Si–B microstructures according to Lemberg et al.^[17] Microstructure optimized for a) maximum oxidation resistance, b) creep resistance, and c) damage tolerance.

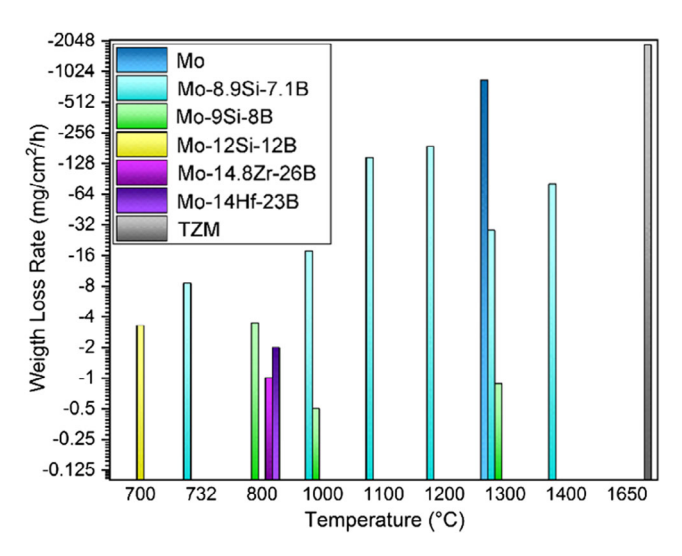


Figure 4. Measured weight loss per hour after oxidation tests of Mo-based alloys (data taken from the previous studies^[9,28,29,41,56,93]). Alloy compositions are given in at%, TZM.

Mo helps to reduce the weight loss; however, the weight loss is still quite high. Therefore, appropriate oxidation protection of the material is necessary.

1.3. Coating Requirements

As the alloys' microstructure can either be optimized with regards to the mechanical properties or the oxidation resistance, a common concept is to optimize the material with respect to the thermo-mechanical properties while considering moderate oxidation properties of the material. The oxidation properties can be improved by a suitable post-treatment, in particular, the application of environmental barrier coatings (EBCs). This strategy allows to combine excellent oxidation resistance and mechanical properties in one component. Due to the complex oxidation kinetics of Mo–(Si–B) alloys, the coating is mainly needed to protect the material against pesting at the temperatures between 700 and 900 °C.

The coating materials must offer a high temperature stability, and this includes high melting temperatures, chemical stability, thermal shock stability, and no phase transitions in the relevant temperature regime. Furthermore, the materials must withstand the aggressive turbine atmosphere, where oxygen, water vapor,

and fly ash (calcium–magnesium–alumino–silicate [CMAS]) are present. Moreover, the coefficient of thermal expansion (CTE) of the coating material should match the substrate, aiming to the reduction of thermal stresses during operation. In addition, the materials' thermal expansion must not be highly anisotropic; i.e., the material must not have different CTEs that apply to different spatial directions, as this can lead to stress and crack formation within the material during heating and cooling phases. An overview of relevant materials and their CTEs is given in **Table 1**.

Another important factor is the coating thickness, which can be affected by the coating process duration or the number of coating runs. Thick coatings are expected to prevent oxidation of the substrate for a longer period. Production of thick coatings is often time-consuming and, therefore, more expensive. However, increasing the coating thickness leads to increased elastic strain energy and, hence, the probability for cracks and coating failure rises.^[22] Otherwise, thin coatings may be insufficient for reliable protection of the material for a long period of time.

Besides the chemical and mechanical resistance of the coating, the coating's microstructure strongly influences the protection efficiency of the coating. In the field of EBCs, dense coatings are preferred, because they form an effective barrier that cannot easily be penetrated by the aggressive gases in the turbine atmosphere. However, dense coatings come along with higher stresses, [23,24] which might reduce the coating lifetime. In contrast to this, porous coatings offer more favorable stress level and stress relaxation properties.^[25,26] In addition, they have lower heat conductivity, which makes them popular in the TBC area, as lower substrate temperatures lead to decreased oxidation rates of the substrate. Nevertheless, oxygen and other reactive fluids can penetrate through open pores and cracks, and this reduces the protection efficiency of porous coatings. The obtained coating microstructure is related to the coating procedure and can be adjusted within certain limits by varying the coating parameters.[27]

As all these factors determine the protection efficiency of an EBC, it is important to find a proper coating system. This may involve compromises in certain properties (e.g., density and thickness). Furthermore, the coating system might require the application of several materials or processes. Thus, effective coating strategies for Mo/Mo-based alloys are still to be found. Different approaches and procedures are currently subject of research, which are summarized as follows.

and-conditions) on Wiley Online Library for rules of use; OA articles are governed by the applicable Creative Commons

ENGINEERING

www.advancedsciencenews.com www.aem-journal.com

Table 1. Overview on CTE of selected materials.

Material	CTE (10^{-6} K^{-1})
Al	26.7 ^[106]
Al_2O_3	8.6 ^[107]
В	5.0-7.0 ^[108]
CaMoO ₄	13.5/22.8 (*) ^{a)[109}
CMAS	9.8 ^[110]
Cr	10.8[111]
CrN	7.16 ^[112]
CrSi ₂	16.8/10.9(*) ^{a)[113]}
$Gd_2Zr_2O_7$	12.4 ^[114]
Мо	5.7 ^[115]
Mo ₂ B	5.0 ^[116]
Mo_2B_5	8.6 ^[116]
Mo ₂ N	6.7 ^[117]
Mo ₃ Si	7.2 ^[118]
Mo ₅ Si _{2.97} B _{0.16}	5.7/13.9 (*) ^{a)[28]}
Mo ₅ Si ₃	11.8/5.8 (*) ^{a)[7]}
Mo ₅ SiB ₂	7.55 ^[57]
МоВ	8.4/6.4 (*) ^{a)[118]}
MoB ₂	7.7 ^[116]
MoSi ₂	8.0/10.0 (*) ^{a)[28]}
Mo–Si–B	5.0-6.0 ^[28]
PHPS (pyrolyzed)	3-4 ^[86,88]
Si	2.6 ^[119]
SiB ₆	5.1 ^[120]
SiC	5.1 ^[121]
Si ₃ N ₄	3.6 ^[122]
SiO ₂	0.5–4.1 ^[28]
Steel (fcc)	17 ^[123]
Ti	10.5 ^[124]
TiN	11.0 ^[125]
W	4.6 ^[126]
YSZ	11.7 ^[127]

^{a)}(*) Marked phases show high CTE anisotropy.

2. Coating Strategies

The formation of MoO₃ must be prevented to avoid degradation of Mo components, and various concepts and preparation methods for this are under discussion. However, they share a common concept: the surface must be treated in such a way that the inward diffusion of oxygen is blocked; on the other hand, outward diffusion of Mo/MoO₃ needs to be minimized.^[9] This surface passivation can be achieved by chemical modification of the samples' surface^[9,15,16] or by application of coatings, which act as diffusion barrier.^[28–34] To maintain the excellent mechanical properties of the material, most approaches favor the application of protective coatings.

Among the different coating concepts, metallic Mo–Si–(B) coatings produced by chemical vapor deposition (CVD),^[35] pack cementation (PC),^[36–40] or magnetron sputtering^[28] are the most prominent approaches. Other approaches, such as MoSi₂ coatings produced by spraying techniques^[41–44] or plasma transferred arc (PTA),^[29] are less frequently studied. Besides this, there are groups that focus more on ceramic coatings,^[33,45] comparable to the frequently used TBC systems. The variety of different coating strategies is summarized in **Figure 5**.

2.1. Surface Passivation by Pre-Oxidation

As discussed in the sections earlier, the oxidation kinetics of Mo-Si-B is complex. These complex oxidation mechanisms enable the possibility to passivate the surface by pre-oxidation. [9,15,16] Pre-oxidation at 1200–1300 °C for 100 h^[16] led to the formation of a dense, continuous silica scale on the surface (\approx 40 μ m) and an inner diffusion zone (20 µm), which consists of Mo and SiO₂ (see Figure 6). This zone is depleted of Mo₅SiB₂ and Mo₃Si. Meyer et al. [8] showed that the depletion is caused by a low oxygen partial pressure ($<5 \times 10^{-11}$ Pa) at the silica–substrate interface, due to the dense silica scale (diffusion-limited oxidation). The low oxygen partial pressure favors the oxidation of Mo₅Si₃ to form SiO₂ and Mo, according to the disproportionation reaction, instead of MoO3 and SiO2 (see Equation (1) and (2)). This disproportionation causes the depletion of the intermetallic phases in the intermediate layer. In addition, the formation of a 40 um thick and dense oxide scale during pre-oxidation hinders degradation of the sample at subsequent oxidation tests at 800 °C. [15] The oxidation tests performed by Burk et al. showed that 100 h of pre-oxidation at 1200 °C is sufficient to suppress pesting behavior at 1200 °C in air for at least 50 h.[8,16]

High
$$O_2$$
 partial pressure (20 KPa):
 $Mo_5Si_3 \stackrel{\Delta T,O_2}{\rightarrow} 5 MoO_3 \uparrow +3SiO_2$ (1)

Low O₂ partial pressure (
$$< 5 \times 10^{-11} Pa$$
):
 $Mo_5 Si_3 \stackrel{\Delta T,O_2}{\rightarrow} 5Mo + 3SiO_2$ (2)

Similar observations were made by Behrani et al. [46] Here, Mo–Si–B alloys were alloyed with Nb to improve their mechanical properties. Nb, however, oxidizes and forms non-volatile Nb₂O₅, which hinders the formation of a continuous silica scale. The samples were pre-oxidized and then subjected to chlorination to remove the Nb₂O₅ by the formation of volatile NbCl₅. Oxidation tests at 1000 °C revealed a weight gain of 1.3 mg cm⁻² after 10 h, which is half of the weight change of an unprotected alloy. Although surface passivation due to pre-oxidation at elevated temperatures seems to improve the oxidation resistance of Mo–Si–B alloys, long-term stability of the system is questionable. [15]

2.2. Metallic Coatings

A common way to increase the oxidation resistance of Mo or Mo-based alloys is to protect the surface by deposition of

arch Center, Wiley Online Library on [01/05/2024]. See the Terms and Condit

of use; OA articles are governed by the applicable Creative Commons

Figure 5. Overview on different coating strategies for Mo-Si-B alloys.

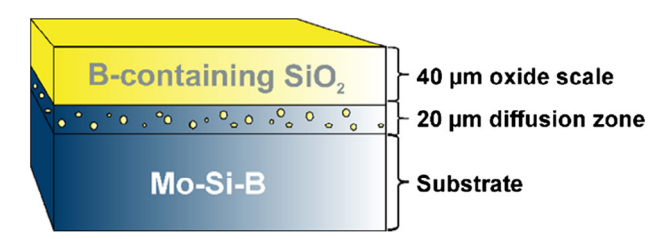


Figure 6. Schematic illustration of Mo–Si–B alloy oxidized for 4 h at $1300\,^{\circ}\text{C}$ (according to Mendiratta et al.^[15]).

oxidation-resistant molybdenum silicides, especially $MoSi_2$. During high-temperature treatment in air, these phases will in situ form protective scales. Metallic coatings can be applied by several methods, such as CVD/physical vapor deposition (PVD), sputtering, and plasma spraying, which will be discussed in the following sections.

2.2.1. Chemical Vapor Deposition

CVD is a general term for several vacuum coating techniques. CVD is commonly used to obtain thin metallic or ceramic coatings on metallic surfaces. The substrate is placed in a process chamber, and one or more gaseous precursors of the coating material are ejected into the chamber. At the substrates surface, the precursor reacts or decomposes to form the desired coating phase. The coating is formed by inward diffusion of the applied metal and formation of mixing phases; therefore, they are called "diffusion coatings." Simultaneous requirement of high temperatures, appropriate saturation atmospheres, and slow

deposition rates makes this process quite complex and expensive. On the other hand, the elaborate process design allows precise control of the resulting coating properties by influencing the coating parameters, for example, coating duration, pack composition, and temperature.

Coating of Mo-based alloys by CVD involves several process steps. First, the sample is nitridated with ammonia at 1100 °C for 2 h. During nitridation, a Mo₂N layer is formed at the surface. The subsequent CVD of Si was carried out using SiCl₄ and H₂ as process gases for 5 h at 1100 °C, leading to the formation of a continuous MoSi₂ coating with $\alpha\text{-Si}_3\text{N}_4$ particles at the grain boundaries (see **Figure 7**). This coating substrate system offers a lower CTE mismatch $^{[47]}$ ($\Delta_{\text{CTE}}=0.7\times10^{-6}\,\text{K}^{-1}$ for MoSi₂ with 40 vol% Si₃N₄) compared with CVD-Si coatings without previous nitridation ($\Delta_{\text{CTE}}=3.1\times10^{-6}\,\text{K}^{-1}$). $^{[35]}$

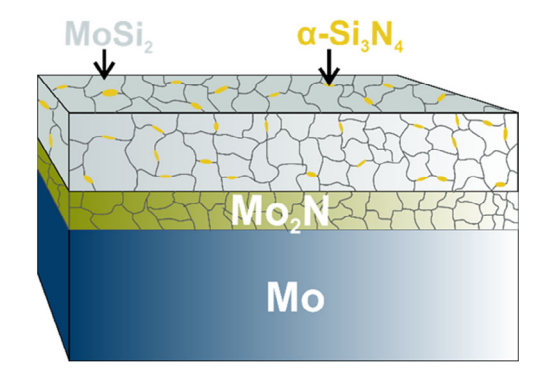


Figure 7. Schematic coating structure of $MoSi_2/\alpha$ - Si_3N_4 composite coating (according to Yoon et al.^[35]).

onditions) on Wiley Online Library for rules of use; OA articles are governed by the applicable Creative Commons

Figure 8. Coating structure and oxidation behavior of (Mo,W)Si₂-Si₃N₄ composite coatings (according to Zhang et al.^[48]).

Similar approaches with implementation of W and Cr were studied. Promising results were published by Zhang et al. [48] The samples were first pack tungstenized, then nitrided with ammonia, and finally pack siliconized. The layer concept is sketched in **Figure 8**. The formed W-containing phases had beneficial impact on the oxidation resistance. Compared with $MoSi_2-Si_3N_4$ and $MoSi_2-CrSi_2-Si_3N_4$ coatings, they provide an increase in oxidation resistance by one order of magnitude (see **Figure 9**). [49]

Si PC: Another widely used CVD technique is the PC process. The sample to be coated is packed tightly together with the metal powder and an inert filler material (alumina) in a sealed crucible.

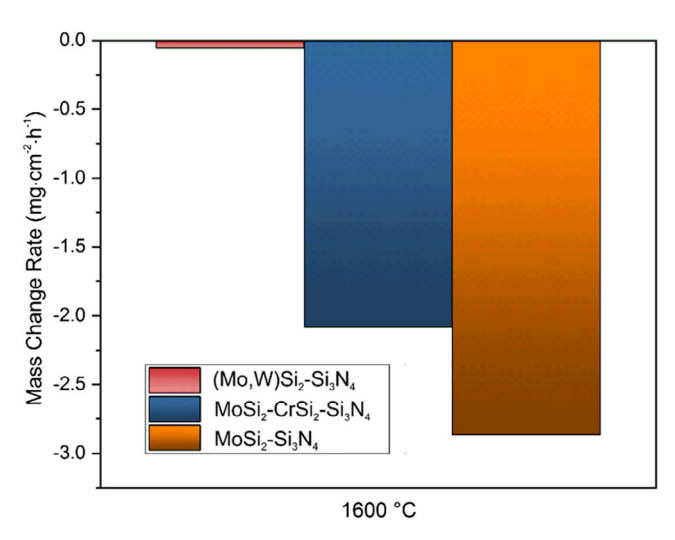


Figure 9. Weight change rates of CVD-MoSi₂-composite coatings during oxidation test at 1600 °C (data from the previous studies^[48,49]).

Halides, such as NaF, HCl, or NH₄Cl, are often used as activator (halide activated PC [HAPC]). The crucible is then heated to temperatures in the range of 700–1500 °C and kept for several hours. During heat treatment, the metal powder reacts with the activator to form gaseous MX (M = metal, X = halide). When the gaseous metal halides reach the substrate, they decompose, and the metal is deposited on the substrate's surface. The deposited metal diffuses into the substrate, and a mixed coating is formed according to thermodynamic equilibria. Due to the growth direction of the coating, the resulting coating offers a columnar microstructure. [50]

Some research groups focus on the deposition of Si on Mo or Mo-based alloys by HAPC. [36–40] Recently, Choi et al. [38] demonstrated the increase in the lifetime of Mo–Si–B alloys after the application of a Si PC coating. After 48 h of coating procedure at 1100 °C, a 58 μm thick MoSi $_2$ coating was obtained. A MoB layer of about 6 μm thickness was found at the interface between MoSi $_2$ and Mo–Si–B. This layer cannot be found in alloys with low B content, [45] and it is believed to prevent further diffusion of Si into the substrate. [51]

A complex layer structure (see **Figure 10**) was found after 40 h of oxidation in air at $1400\,^{\circ}$ C. [^{38]} During the oxidation test, a 10 µm silica scale was formed, which serves as oxygen diffusion barrier. The formation of the silica scale leads to a depletion of Si in the MoSi₂ layer. As a consequence, a 10 µm thick Mo₅Si₃ layer was formed in between the silica scale and the MoSi₂ layer. Si diffusion through the MoB layer into the substrate leads to the formation of a second Mo₅Si₃ layer underneath the MoSi₂ layer. After 40 h of oxidation test, the coated sample showed a weight decrease of $\approx 0.07\%$. For comparison, the uncoated alloy showed a weight loss of 66.2% after only 5 h. [^{38]}

The long-term behavior of these coating system was studied by Cox and Brown. $^{[36]}$ They demonstrated that an 80 μm thick silicide coating on Mo is able to pass six month of static oxidation test at 1000 °C. The observed coating structure was similar to the one reported by Choi et al., $^{[38]}$ although a non-B-containing substrate was used. The layer structure is sketched in Figure 10, bottom. After coating production, a thin Mo₅Si₃ layer is observed instead of a MoB layer. During oxidation, a SiO₂ and a Mo₅Si₃ layer are formed on the sample's surface, resulting in a coating structure similar to that promoted by the Mo–Si–B alloy, except for the MoB layer. With ongoing oxidation, the MoSi₂ layer is consumed and fully replaced by a continuous Mo₅Si₃

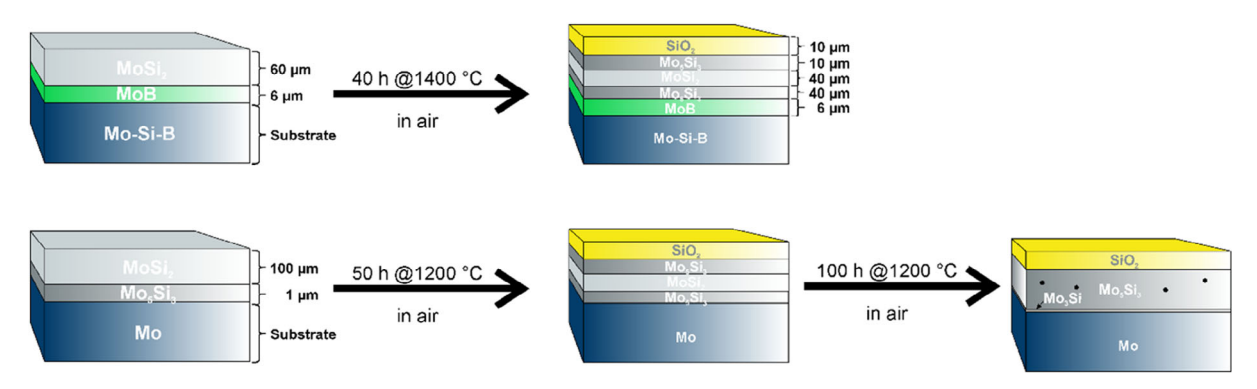


Figure 10. Schematic illustration of the coating structure of Si pack cemented coatings on Mo–Si–B (top, according to Choi et al.^[38]) and Mo (bottom, as described by Cox and Brown^[36]), before (left) and after oxidation test (right).

ADVANCED ENGINEERING MATERIALS

www.advancedsciencenews.com www.aem-journal.com

layer. In addition, due to the ongoing Si depletion, the formation of a Mo_3Si layer is observed below the Mo_5Si_3 layer. [39] As result of the high Si diffusion, Kirkendall voids are observed. [52]

To increase the oxidation resistance of Mo-based alloys, attempts were made to add additives to the powder pack. For this purpose, Sun et al.^[53] studied the effect of particulate fillers (Al₂O₃, SiC, and SiO₂) on the oxidation resistance of MoSi₂ coatings. The coatings with SiC fillers showed the lowest weight change after oxidation at 500 °C; coatings with SiO₂ fillers showed the highest oxidation resistance at 1200 °C, which was attributed to the formation of a protective SiO₂ scale at the surface. Majumdar^[54] and Zhang et al.^[55] demonstrated that the addition of aluminum can increase the oxidation resistance of the coating, due to the formation of a fast growing alumina scale. Sakidja et al.^[56] showed that PC of Al (without Si) leads to a similar layer concept as the Si PC. The deposited coatings showed an excellent oxidation resistance and a weight gain of only 2.35 mg cm⁻² after oxidation at 1300 °C for 50 h.

Si + B PC: As already known from the development of Mo–Si–B alloys, adding B can help to establish a protective silica scale. Therefore, the deposition of Si- and B-containing coatings was studied in detail by several research groups. In principle, there are two different ways to deposit pack-cemented Si and B coatings. One method is the so-called co-deposition, in which both are simultaneously deposited on the substrate. The other method is the two-step process, in which one is deposited first and then the other. The resulting coating consists of two layers, which will diffuse into each other during heat treatment. [34,45,51,57–62]

The deposition of B and Si in a two-step process was in focus of several investigations. [57,61,62] The samples were first boronized and then siliconized. Two layers were obtained after coating procedure: an inner MoB layer and an outer MoSi₂ layer (see **Figure 11**). As already mentioned, the main coating formation mechanism is inward diffusion of Si and B. After the oxidation test several layers have formed due to diffusion and oxidation, underneath the MoB layer, the formation of a

 Mo_2B layer is observed, which is explained by the ongoing inward diffusion of B. Two newly formed layers are found in between the $MoSi_2$ and the MoB layer: a mixed layer of Mo_5SiB_2 and Mo_3Si , and a Mo_5Si_3 layer adjacent to the $MoSi_2$ layer. $^{[61]}$ Mo_5Si_3 dispersions have formed in the $MoSi_2$ layer, and a small Mo_5Si_3 layer was observed between the $MoSi_2$ and the oxide scale (see Figure 11).

Comparative studies by Wang et al. showed an increased lifetime of Si + B coatings in contrast to Si pack-cemented coatings. This increase in lifetime is attributed to the formation of Mo₅SiB₂ and MoB phases. The diffusion coefficient of Si in Mo₅SiB₂ (1.7 × 10⁻¹³ cm² s⁻¹) is three orders of magnitude lower compared with Mo₅Si₃ (4.1 × 10⁻⁹ cm² s⁻¹). [63] Consequently, the mixed layer (Mo₅SiB₂ + Mo₃Si) acts as a kinetic bias against Si inward diffusion. It is believed that the MoB phase further enhances this effect.

The co-deposition of Si and B has been intensively studied by Perepezko et al. and Lange et al. [34,45,51,58,59] A mixed powder bed of Si + B was used for coating deposition. The layer structure resulting from the co-deposition process is comparable to that one obtained by the two-step process. After the co-deposition. a thin (10 µm) MoB and a thicker (100 µm) MoSi₂ layer with small dispersions of MoB are observed (see Figure 12). In addition, a very thin (2 µm) Mo₅Si₃ layer is found at the interface between MoSi₂ and MoB. Furthermore, a thin (1 µm) Mo₂B layer has formed in between the substrate and the MoB layer. During oxidation, a silica scale is formed on the surface. The MoB dispersions in the MoSi₂ phase promote the formation of a dense oxide scale, leading to an increased oxidation resistance. The MoSi₂ layer is consumed with ongoing oxidation, leading to the formation of a Mo₅Si₃ layer in between the silica and the MoSi₂ layers. The formed MoB and Mo₂B layers act as diffusion barriers against the inward diffusion of Si; as a consequence, a Mo₅SiB₂ layer is formed at the interface between Mo₅Si₃ and MoB. This additional Mo₅SiB₂ layer acts as Si reservoir and decelerates the conversion from MoSi₂ to the low oxidation-resistant

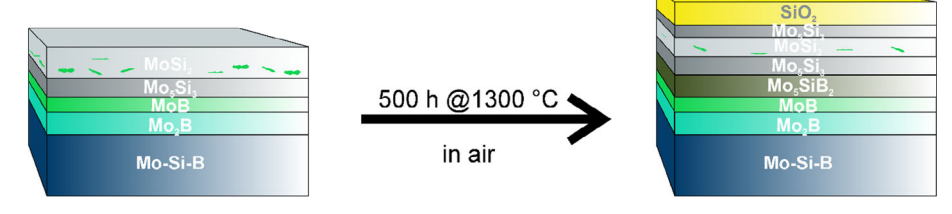


Figure 11. Schematic representation of the layer concept of pack-cemented coatings on Mo–Si–B manufactured by two-step deposition of B and Si (data from Wang et al.^[61]).

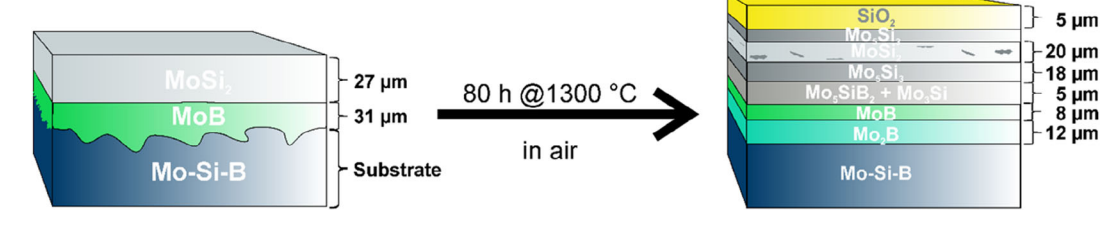


Figure 12. Schematic representation of the layer concept of pack-cemented coatings on Mo–Si–B manufactured by co-deposition of Si and B, as described by Tian et al.^[60]

szentrum Jülich GmbH Research Center, Wiley Online Library on [01/05/2024]. See the Terms

nditions) on Wiley Online Library for rules of use; OA articles are governed by the applicable Creative Commons

www.aem-journal.com

Mo₅Si₃ phase (see Figure 12).^[60] In contrast to the studies with two-step deposition of Si and B, a continuous Mo₅SiB₂ layer is formed in this case. This layer might have an increased impact on the Si inward diffusion compared with the mixed layer.

The resistance of pack-cemented Si + B coatings against water vapor and CMAS attack was investigated by Downs et al. [64] and Perepezko.^[34] The results show that the dense borosilicate-glass scale offers a good resistance against water vapor attack. The CMAS that was applied on the surface reacted with the silica scale. Consequently, SiO₂ and MoO₂ were formed. The MoO₂ reacts with Ca from CMAS to form CaMoO₄, which crystallizes on the surface (see Figure 13). As a result, the CMAS slag is depleted from Ca, and this increases the viscosity of the slag and prevents the sample from further corrosion. [34]

Tang et al.^[57] compared the different PC strategies, such as Si-only coatings, Si + B two-step deposition, and Si + Bco-deposition. Oxidation tests have shown that borosilicide (Si + B) coatings offer a higher resistance to oxidation than Si-only coatings. This is in accordance with the analysis of the oxidation test results of the various PC coating strategies, which are visualized in Figure 14.

The Si + B coatings are sufficient to protect the material up to 1100 °C for thousands of hours. This impressive lifetime decreases dramatically with increasing temperature, resulting in an average lifetime of several tens of hours at 1600 °C. [57] The main reason for this decrease in lifetime is the fast-inward diffusion of Si and the associated formation of the T1 (Mo₅Si₃) phase. This leads to the conclusion that Si depletion through the formation of the oxidation-prone T1 phase is the life-determinant factor of MoSi₂ coatings. This fosters the need for more effective coating strategies and better Si diffusion barriers.

2.2.2. Molten Salt

A different coating strategy is the molten salt technique, which has been studied by Suzuki et al.[31] MoSi₂ coatings are produced by an electroless plating technique. In this case, a salt mixture of NaCl, KCl, NaF, Na₂SiF₆, and Si is heated to 700-900 °C. The mixture starts to melt at around 650 °C. The Mo substrates were suspended into the melt for several hours. Si starts to

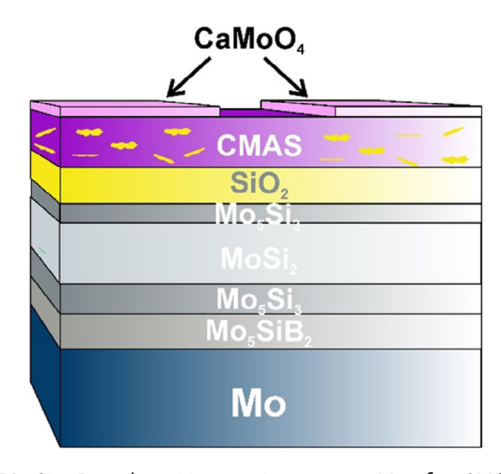


Figure 13. Si + B co-deposition coating on pure Mo after CMAS attack (with reference to Downs et al. [64] and Perepezko [34]).

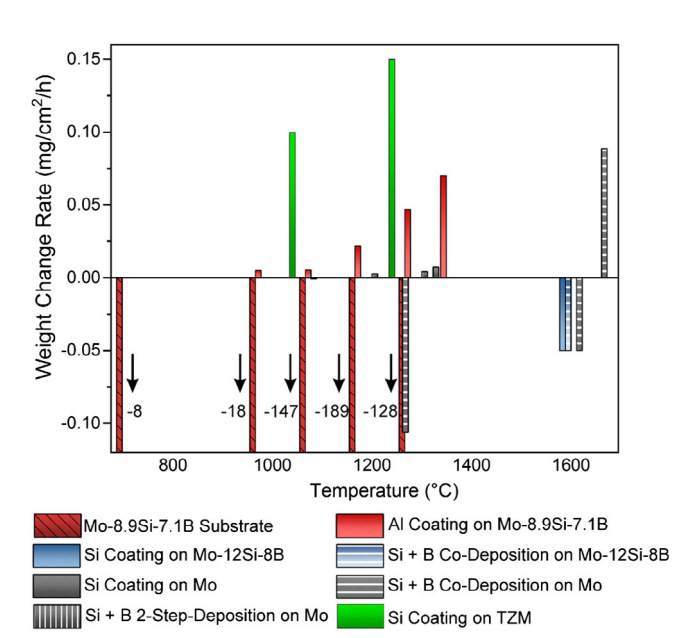


Figure 14. Weight change rates of different PC coating systems on Mo-based substrates (data from the previous studies[34,37,38,56-58,60-62]).

diffuse into the substrate, and a coating is formed on the samples surface.

Such as in the PC process, the main mechanism of coating formation is the inward diffusion of Si, which leads to the formation of a continuous MoSi₂ layer. Due to the fast deposition rate, no Mo₅Si₃ layer is present immediately after coating. The reaction scheme of the redox reaction is shown in Equation (3) and (4).

Oxidation
$$Si + 6F^- + SiF_6^{2-} \rightarrow 2SiF_6^{4-}$$
 (3)

Reduction
$$2SiF_6^{4-} + Mo \rightarrow Mo - Si + 6F^- + SiF_6^{2-}$$
 (4)

The coating structures of samples directly after coating procedure and after oxidation test are shown schematically in Figure 15. The MoSi₂ coatings produced by molten salt synthesis can suppress pesting at low temperatures; however, at high temperatures, Mo₅Si₃ is formed at the interface. The same layer structure as for the Si pack-cemented coatings was found after oxidation in air. A major drawback of this process is the slow growth rate of the MoSi₂ layer on the sample edges, which led to severe damage due to oxidation of the Mo substrate.

2.2.3. Liquid Siliconizing

Zhang et al. [32] demonstrated the feasibility of the liquid siliconizing process to produce Si-MoSi₂ functionally graded coatings on Mo substrates. The substrates were inserted into the molten silicon at 1460 °C for 20 min in Ar atmosphere. The coating is, again, formed by inward diffusion of Si and shows the wellknown MoSi₂ and Mo₅Si₃ + Mo₃Si layer structure. The formed coatings show the typical columnar microstructure, they are dense, and no microcracks are observed. The MoSi2 columns are found embedded in a Si matrix, leading to a high Si content

15272648, 2021, 4, Downloaded from https://onlinelibrary.wiley.com/doi/10.1002/adem.202001016 by Forschungszentrum Jülich GmbH Research Center, Wiley Online Library on [01/05/2024]. See the Terms

nditions) on Wiley Online Library for rules of use; OA articles are governed by the applicable Creative Commons

Figure 15. Schematic illustration of MoSi₂ coatings on pure Mo substrates produced by molten salt according to Suzuki et al.^[31]

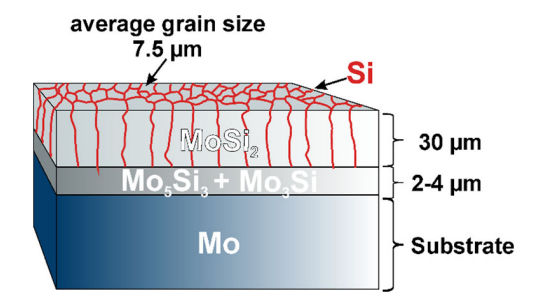


Figure 16. Schematic drawing of Si–MoSi₂ coatings on pure Mo substrates (data from Zhang et al.^[32]).

in the coating (see **Figure 16**). The Si–MoSi $_2$ coatings were subjected to oxidation tests at 1600 °C. After 70 h, the samples showed only a weight gain of 0.17 wt%, and this is quite low compared with pure Mo and MoSi $_2$. The excellent oxidation resistance of these Si–MoSi $_2$ coatings was attributed to the high Si content in the coating.

The elemental Si in the coating acts as a silicon reservoir, preventing excessive formation of Mo_5Si_3 . As a result, the oxidation resistance of coatings produced by liquid siliconizing is enhanced. A further advantage of this technique is the increased coating thickness and reduced coating process duration compared with the molten salt technique and the CVD process, respectively.

Major disadvantages of this process are the high temperatures and the associated high energy consumption. Although the coating time is relatively short compared with the CVD process, the process, however, is still time-consuming.

2.2.4. Sputter Deposition

Metallic coatings can also be produced using the sputter deposition process. For this purpose, one or more so-called targets are installed, which contain the desired coating material. Only conductive materials can be used as target material, because they act as cathode in this process. The substrate to be coated is placed in a vacuum chamber at a defined distance below the target. To avoid oxidation during the process, the chamber is purged several times with an inert gas (usually argon). The applied voltage is used to generate a (argon) plasma. Collisions with the plasma ions cause the ejection of atoms or particles from the target into the gas phase. Afterward, the ejected gas particles condense on the substrate, and a coating is formed. The different sputtering techniques differ in the electric field application, for example, direct current (DC) sputtering and radio frequency (RF) sputtering. Another sub-process is magnetron sputtering, where a magnetic field is generated in addition to the electric field.

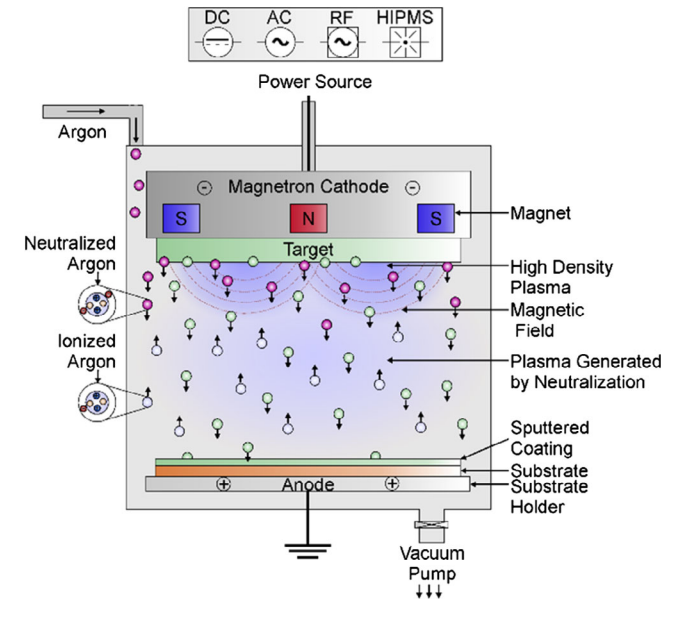


Figure 17. Schematic drawing of the magnetron sputtering process (adapted from the previous study^[97]).

This influences the movement of the charge carriers in the chamber, allowing more particles to be ejected from the target, resulting in higher sputtering rates. A schematic illustration of the magnetron sputter process is presented in **Figure 17**.^[65]

Sputtering is an advanced coating technique that allows to influence the coating properties precisely by controlling the coating parameters, such as temperature and pressure. As almost all conductive materials can be used as a target and several targets can be used simultaneously, the process has a high flexibility. In addition, almost every solid material can be used as a substrate. A further advantage is that the ejection into the gas phase is not thermally induced, so that no demixing effects occur even when alloys are processed. However, the process is very complex, as the process chamber must be under vacuum during sputtering. The necessity of a vacuum coating chamber makes it more complicated to coat large components. Coating of parts with complex geometries is problematic, because the material transport occurs directly from the target to the substrate; thus, undercuts cannot be coated or not homogeneously coated. Furthermore, the obtained coatings are very thin despite long coating durations. In addition to that, the deposited coatings are often amorphous.^[66] Volume changes during the heatinduced crystallization processes during service can induce mechanical stress from thermal mismatch, which may cause coating spallation.

ditions) on Wiley Online Library for rules of use; OA articles are governed by the applicable Creative Commons

www.aem-journal.com

Lange et al.^[28,30] and Govindarajan et al.^[67] studied the deposition of thin Mo–Si(–B) coatings on Mo–Si–B alloys by magnetron sputtering. The deposited coatings offer a columnar microstructure, which is typical for sputtered coatings. Both studies suggest to introduce an interlayer between coating and substrate to prevent Si inward diffusion and, thus, formation of sub-silicides. However, the use of Ti, TiN, Cr, and CrN as diffusion barriers, which was studied by Govindarajan et al,^[67] has not proofed to be beneficial, as they were not able to prevent the Si-inward diffusion.

A more promising concept is the deposition of several (10–50) Mo/Si multilayers. $^{[67]}$ The concept of Lange et al. $^{[28]}$ involved the deposition of a 2 μm Mo $_5 SiB_2$ interlayer before coating of the samples with Mo–Si–B coatings (5 μm). The schematic layer concept is presented in **Figure 18**. The samples were subjected to oxidation tests at 800, 1000, and 1300 °C. It was found that coatings with high boron content offer best oxidation protection at 800 °C. However, with increasing temperature, enhanced oxidation resistance was observed for coatings with lower boron content. Nevertheless, the results show that even 7 μm thin coatings are sufficient to protect the material against oxidation for more than 100 h.

Lange et al.[30] further developed this coating strategy: Mo-Si-B alloys were coated with 5-10 µm thick sputtered layers of Mo-Al, Mo-Si-B, or Mo-Si-Al. The deposited layers serve as a combined oxidation barrier and bond coat. In some cases, an additional diffusion barrier (Mo₅SiB₂, 2 µm) was added between substrate and bond coat. Afterward, the samples were pre-oxidized, leading to the formation of aluminum borate, borosilicate, and mullite scales, respectively. This protective oxide scales offered a well adhering surface for the following top coats. Yttria-stabilized zirconia (YSZ) or Gd₂Zr₂O₇ coatings with 145-160 µm thickness were applied as additional TBCs by electron beam PVD (EB-PVD). Oxidation tests of these samples revealed a satisfying oxidation protection for short-term use (20 h), but oxidation for more than 100 h or at 1300 °C led to severe damage of the sample, so that there is still room for improvement. The premature failure of these coating systems might be attributed to the high CTE differences within the system.

The weight change rates of the different coatings are summarized in **Figure 19**. It is obvious that the coatings can significantly

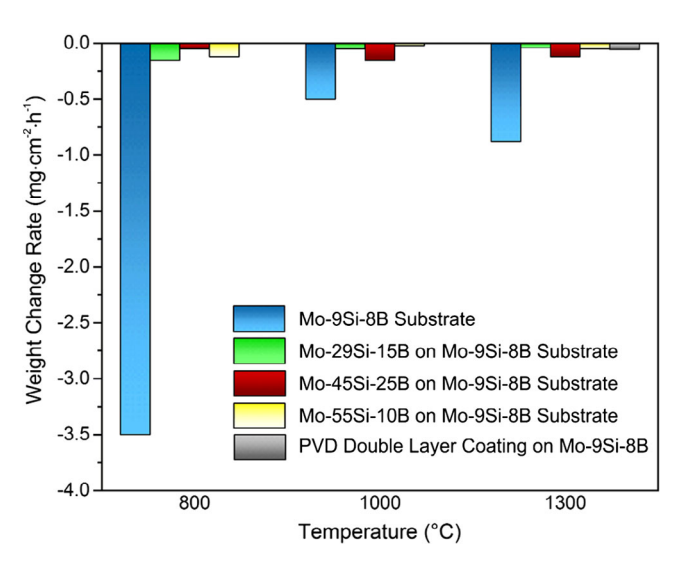


Figure 19. Weight change rates of sputter-coated samples during oxidation at various temperatures (data from the previous studies^[28,30]).

reduce the Mo pesting during oxidation tests. Despite this, no further decrease is observed when a PVD top coat is used. However, the long-term oxidation resistance needs to be drastically increased, and this may be achieved by increasing the coating thickness. Low deposition rates of $<1\,\mu m$ per hour during sputtering make it difficult to increase the coating thickness within a reasonable coating duration. This makes the sputter process time-consuming and difficult to implement on an industrial level.

2.2.5. Spray Processes

Alongside the above-mentioned coating processes, there is a variety of other coating techniques, such as spraying methods. Coatings produced by spraying processes, for example, slurry spaying or atmospheric plasma spraying (APS), are less time-consuming and more cost-effective compared with sputtering or CVD. Coatings with thicknesses of several hundred micrometers can be achieved within minutes using the spraying

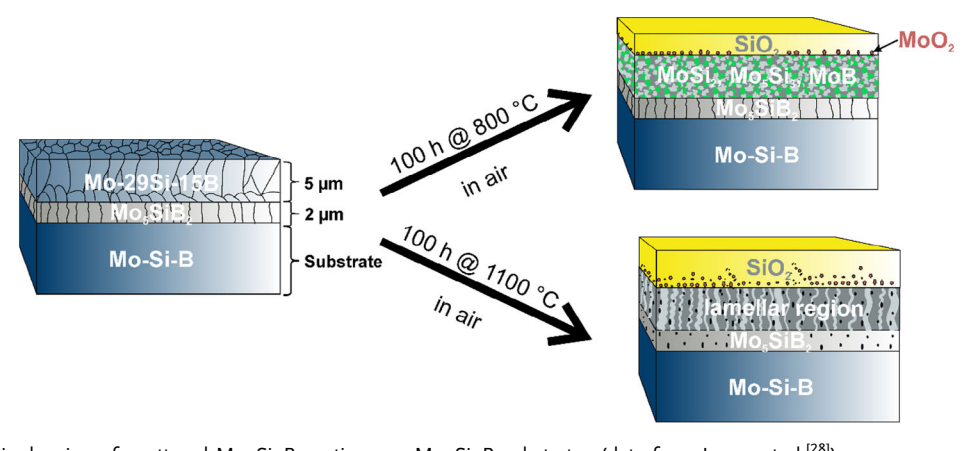


Figure 18. Schematic drawing of sputtered Mo-Si-B coatings on Mo-Si-B substrates (data from Lange et al. [28]).

ADVANCED ENGINEERING

www.advancedsciencenews.com www.aem-journal.com

processes.^[2] Moreover, spraying processes provide high flexibility regarding the spray material and the shape of the component to be coated. Usually, the coating process can be carried out without additional heating of the components, which again makes spray coating more efficient. As diffusion has only a minor effect on coating formation and adhesion, a proper surface treatment must be carried out before spraying to achieve good adhesion properties and long service life. This additional step might involve surface roughening (usually sandblasting) and/or application of bond coats.^[68]

A well-known spraying process is slurry spraying, [69] which involves spraying of a solution or suspension onto a substrate with a spray gun. Apart from that, there is a variety of thermal spray processes. In all these processes, a flame or plasma is used to fuse the spray material. The droplets are then accelerated toward the substrate by a carrier gas flow. Organic, metallic, and ceramic materials can be used as feedstock; furthermore, liquids, suspensions, powders, and wires can be used. The processes differ in the way the flame/plasma is generated, in the used atmosphere and the used spraying nozzles.^[70]

The most prevalent thermal spray process is the APS, which is commonly used in the TBC area. A schematic sketch of a spraying gun and the spraying process is shown in Figure 20. A plasma (Ar, He, or N₂) is generated by electric discharge. With the help of carrier gases, the spray material is injected into the plasma plume, which can reach temperatures above 10 000 °C. The spray material melts and is accelerated toward the substrate, where it resolidifies. This creates a unique coating microstructure of individual splats (re-solidified particles), partially molten splats and enclosed pores. The coating properties can be influenced by variation of the coating parameters, such as plasma gases, coating distance, substrate temperature, and particle size of the spray material. APS owes its name to the fact that the coating process takes place under atmospheric conditions. The disadvantage of atmospheric conditions is that the substrate or the spray material may oxidize during the coating process.

A variation of the APS process is the vacuum plasma spraying (VPS); hereby, the coating process takes place in a vacuum chamber. High-power pumps are needed to create stable process conditions, which makes VPS less time and cost efficient compared with APS. However, it is used when the feedstock material or the substrates are sensitive to oxidation. Furthermore, the

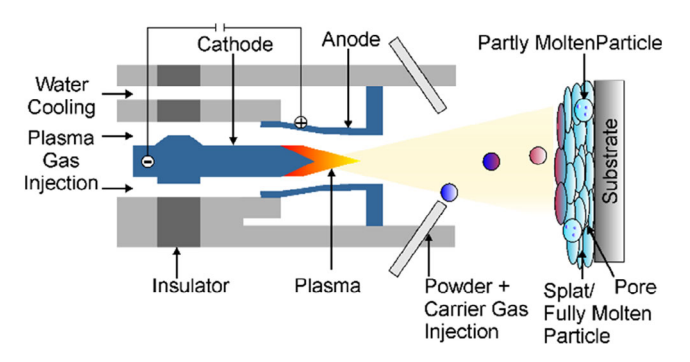


Figure 20. Schematic drawing of a plasma gun and the APS process (a combination of the previous studies^[98,99]).

reduced pressure influences the cooling rates of coating and substrate, leading to reduced thermal stress within the coating.

Another process belonging to the thermal spray family is high velocity oxy fuel (HVOF) spraying. A flammable liquid (kerosene) or gas (methane, H_2) is used as heat source. The expanding combustion gases flow through a Laval nozzle, and the gas velocities of $2000\,\mathrm{m\,s^{-1}}$ are typical. These high velocities lead to increased densification of the resulting coatings. Due to the use of combustion processes as heat source, the maximum process temperature is limited (around $3000\,\mathrm{^{\circ}C}$). This hinders melting of large particles and materials with high melting temperatures. A further disadvantage is the high oxygen content of the obtained coatings.

The protective effect of slurry sprayed coatings on Mo-based alloy containing additions of Zr and Ti (TZM) was studied by Cai et al.^[41] First, an ethanolic slurry of Mo and Si powders was prepared by ball milling and was then sprayed on sandblasted TZM samples. The coated samples were then sintered in argon. Oxidation tests were carried out in air at 1650 °C. After 14 h, large cracks had formed, which led to coating failure (see **Figure 21**).

A more successful coating approach was studied by Jéhanno et al. [42] APS of powder mixtures of Si and B led to protective SIBOR coatings. These about 130 µm thick coatings resisted 30 h of oxidation in air at 1650 °C. This remarkable oxidation resistance can be attributed to the formation of a continuous borosilicate-glass scale, which inhibits oxidation of the inner parts. There are also several studies on MoSi2 coatings manufactured by APS. [43,71,72] Due to oxidation of the MoSi₂ powder during spraying, Mo₅Si₃ and SiO₂ are formed.^[72] A network structure of MoSi₂ and Mo₅Si₃ has formed in the coating (see Figure 22). [43] The formation of Mo₅Si₃ is not favorable, as Mo₅Si₃ additions in MoSi₂ reduce the oxidation resistance of the coating. [7] Furthermore, MoSi₂ in tetragonal and hexagonal crystal structure modifications was found. No protective silica scale was formed during plasma spraying, but 25 h of oxidation at 1200 °C led to the formation of a thin protective SiO₂ scale. The formation of Mo₅Si₃ can be minimized using VPS. A comparative study by Fei et al.^[71] confirmed the higher oxidation resistance of freestanding MoSi₂ coatings prepared by VPS, compared with APS coatings. Nomura et al. [73] studied the suitability of Mo-Si-B coatings produced with very low pressure plasma spraying (VLPPS). Multiphase Mo-Si-B coatings with the same phase constituents (Mo₅Si₃, Mo₃Si, and Mo₅SiB₂) as in the feedstock powder were obtained. Due to the rapid quenching during thermal spraying, nanostructured Mo-Si-B coatings with eutectic composition (Mo-24.5 mol% Si-6.3 mol% B) were formed.^[73]

The formation of oxidation-resistant $MoSi_2$ coatings prepared by HVOF spraying and VLPPS was reported by Reisel et al., ^[44] and a significant influence of the porosity of the thermally sprayed coatings on the oxidation resistance was highlighted. Oxidation tests between 500 and 1500 °C showed that dense coatings offer a higher stability against oxidation.

The results of oxidation tests of $MoSi_2$ coatings obtained by APS and slurry spraying are shown in **Figure 23**. The results show that also porous sprayed coatings can suppress Mo pesting, even at high temperatures.

15272648, 2021, 4, Downloaded from https://onlinelibrary.wiley.com/doi/10.1002/adem.202001016 by Forschun

2arch Center, Wiley Online Library on [01/05/2024]. See the Term

on Wiley Online Library for rules of use; OA articles are governed by the applicable Creative Commons

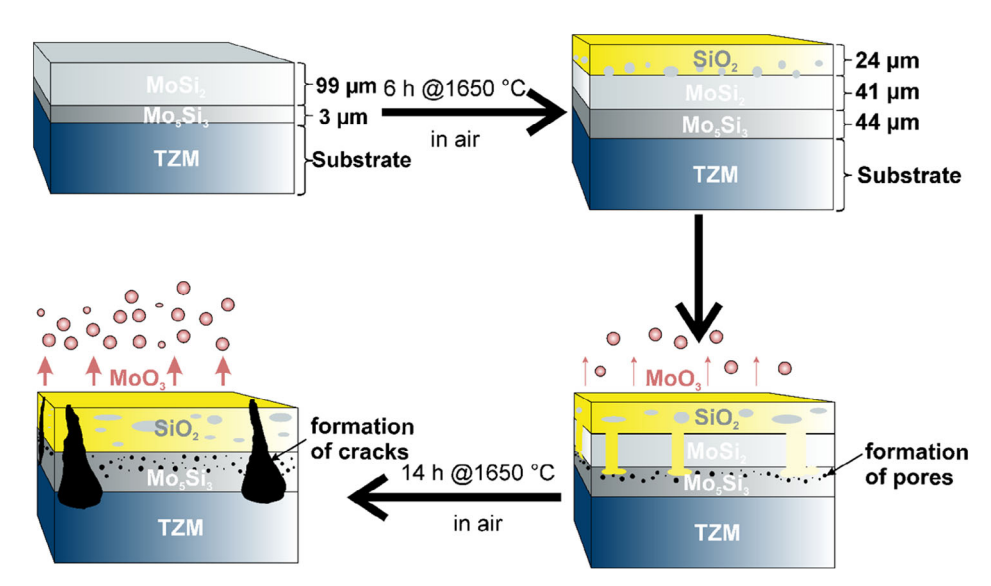


Figure 21. Schematic representation of the oxidation behavior of slurry sprayed MoSi₂ coatings on TZM during 14 h at 1650 °C according to Cai et al. [41]

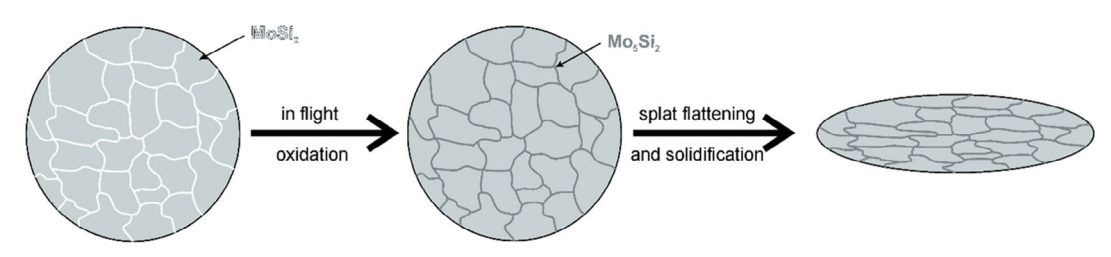


Figure 22. Schematic drawing of coating formation of MoSi₂ during APS (adapted from Yan et al.^[43]).

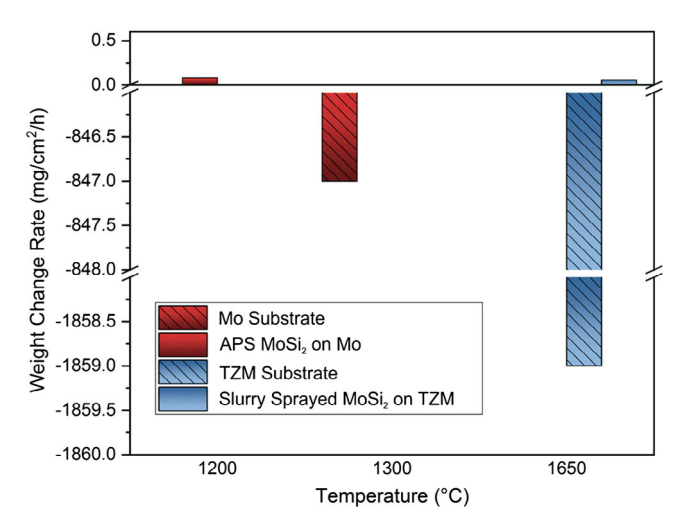


Figure 23. Comparison of the oxidation behavior of $MoSi_2$ coatings obtained by APS and slurry spraying (data from the previous studies^[41,72]). Please note the interrupted scale bar.

2.2.6. Plasma Transferred Arc

A somewhat unusual technique for coating preparation is PTA welding. PTA is a welding process, where the metallic substrate surface is heated by a plasma arc, and (metal) powder is injected

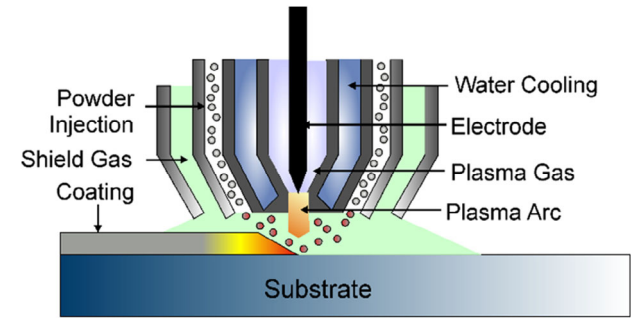


Figure 24. Schematic drawing of the PTA process (in adaption to the previous study $^{[100]}$).

into the arc and melted onto the surface (see **Figure 24**). The obtained coatings offer high adhesion strength, as they are metallurgically bonded to the substrates. Using this technique, coatings with several hundred micrometers in thickness can be produced in a short period of time (up to 20 kg h^{-1}). [74]

In a recent study, Deng et al. [29] investigated the deposition of Mo–Si–B coatings on pure Mo by PTA. A 6 mm thick coating was obtained, which consisted of the same three phases as the original powder: Mo_3Si , Mo_5SiB_2 , and Mo_5Si_3 . The coating mainly consisted of Mo_5SiB_2 and Mo_3Si eutectics with dispersions of Mo_5SiB_2 dendrites and Mo_5Si_3 phase. A 60– $80\,\mu m$ thick,

15272648, 2021, 4, Downloaded from https://onlinelibrary.wiley.com/doi/10.1002/adem.202001016 by Forschungszentrum Jülich GmbH Research Center, Wiley Online Library on [01.05/2024]. See the Terms and Condi

ons) on Wiley Online Library for rules of use; OA articles are governed by the applicable Creative Commons

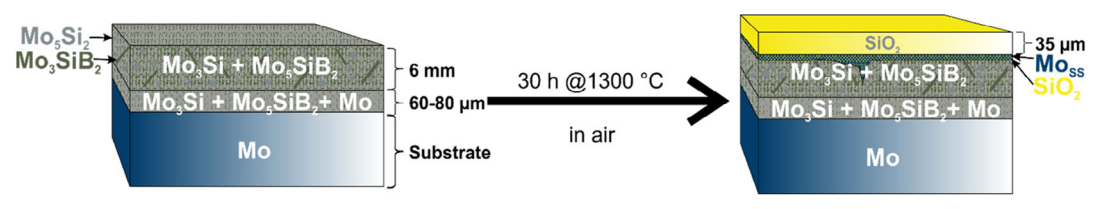


Figure 25. Schematic representation of the microstructure of Mo–Si–B coatings produced by PTA, directly after coating (left) and after exposure to air at 1300 °C (right) (data from Deng et al.^[29])

transitional layer between coating and substrate indicated diffusion bonding. A schematic drawing of the observed layer structure is shown in Figure 25.

The weight loss of the coated sample after 30 h of oxidation at $1300\,^{\circ}\text{C}$ was $-8.2\,\text{m}\,\text{g}\,\text{cm}^{-2}$, resulting in a calculated weight loss rate of $-0.27\,\text{mg}\,\text{cm}^{-2}\cdot\text{h}^{-1}$. In contrast, oxidation tests of the pure Mo-substrate revealed a weight loss of $-141.2\,\text{mg}\,\text{cm}^{-2}$ within $10\,\text{min}$, leading to a calculated weight loss rate of $-847.5\,\text{mg}\,\text{cm}^{-2}\,\text{h}^{-1}$. The excellent oxidation resistance of the coated samples was attributed to the formation of a dense and continuous protective borosilicate scale. This scale was found to heal cracks that occurred in the coating during deposition. [29]

Summary Metallic Coatings: Application of metallic and metalloid coatings is a common way to increase the oxidation resistance of Mo or Mo-based alloys. The deposition of silicon, boron, and/or oxidation-resistant molybdenum silicides was found to have beneficial impact on the oxidation resistance. Diffusion of components of the metallic/metalloid coatings into the substrate leads to the formation of several layers with different compositions. It was found that the Mo₅Si₃ phase is the Mo-Si intermetallic phase most susceptible to oxidation, and that its formation is the life-determining factor; consequently, the formation of Mo₅Si₃ should be avoided.^[7,75,76] Advantages of these coatings are the high coating density and the generally good adhesive strength that results from diffusion bonding. Common feature of the metallic coatings is that protective oxide scales are formed in situ on the surface under oxidizing conditions. It was found that the addition of boron helps to modify the viscosity of the oxide scale to form a covering, dense, and, thus, protective scale, which can heal cracks. [29]

There are several ways to deposit these coatings, and the most common techniques are vapor deposition processes, such as CVD^[35] (especially PC^[34,45,51,57-62]) or sputtering. [28,30] These methods allow precise control of the layer thickness and properties, but a technologically complex setup is required, and the deposition rates are rather low. Pack cemented Si + B coatings showed impressive lifetimes of thousands of hours at 1100 °C; however, the service life is drastically reduced with increased temperature. [57] Higher coating thicknesses ($\approx 100~\mu m$) were achieved by spraying processes $^{[41,72]}$ and PTA welding. [29] But, there are only studies on oxidation behavior up to 30 h between 500 and 1650 °C.

2.3. Ceramic Coatings

2.3.1. Spray Deposition

Besides coating of Mo-based alloys with metallic coatings that form protective oxide scales, the direct application of ceramic coatings was studied as well. For example, Perepezko et al. $^{[45]}$ studied the performance of powder sprayed SiO $_{\!2}$ coatings on Mo–Si–B alloys. The coatings showed good oxidation protection during exposure to air at 1200 $^{\circ}\mathrm{C}$ for 100 h.

As those ceramic coatings are not fully dense, the formation of a borosilicate and a MoO_2 layer in between coating and substrate was observed. It was found that the silica coating can reduce the layer thickness of this intermediate oxide layer by $\approx 50\%$. A further improvement was achieved using an amorphous silica coating, which inhibits the formation of the MoO_2 layer (see **Figure 26**). The amorphous coating was found to be significantly denser compared with the crystalline one.

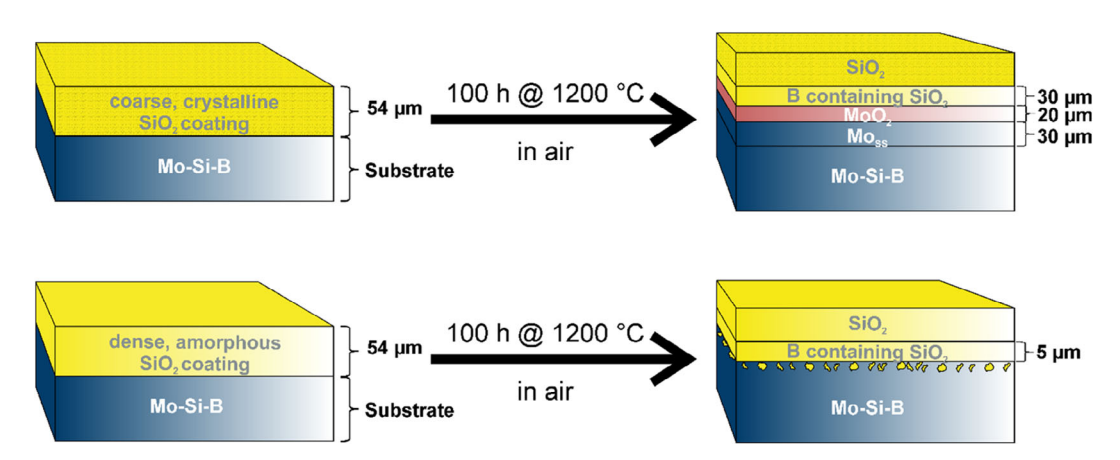


Figure 26. Schematic drawing of powder sprayed dense SiO₂ coating on Mo–Si–B before and after thermal treatment (according to Perepezko et al. [45])

ons) on Wiley Online Library for rules of use; OA articles are governed by the applicable Creative Commons

www.aem-journal.com

2.3.2. Dip Coating with Pre-Ceramic Polymers

Coatings based on polymer-derived ceramics (PDCs) have been proved to hinder oxidation of steel at high temperatures. [77] PDCs are ceramic materials that are derived from a polymeric precursor. Synthetic metal-organic polymers, for example, polysiloxanes, polycarbosilanes, and polysilazanes, act as precursors.^[78] The ceramic precursor can be solubilized, and this offers various possibilities for coating manufacture, for example, painting, dip coating, spin coating, or spraying.^[79] Furthermore, components of different shapes can be coated using PDCs, which makes this strategy versatile. After the coating process, the component is subjected to a drying and cross-linking process at low temperatures (100–400 $^{\circ}$ C) in air. In this step, residues of the solvents are removed, and the cross-linking process enables the transformation of the viscous polymer into a solid coating. A high degree of cross-linking is important to prevent the evaporation of components with low molecular weight during pyrolysis. Depending on the type of polymer used, cross-linking takes place via radical polymerization, polycondensation, transamination, or hydrosilylation. [78] Afterward, the component is subjected to pyrolysis at 700–1400 °C to remove the organic parts and to convert the polymer into Si-O-N(-C)-containing ceramic material. The pyrolysis is typically carried out under protective atmosphere, for example, N₂ or Ar atmospheres. The chosen atmosphere can have an effect on the resulting coating properties and composition; e.g., the formation of nitrides is favored when pyrolysis is carried out in nitrogen atmosphere. [80] In the past, the PDC process route has been used to produce Si-O-N(-C)-containing ceramic at low temperatures.^[81] The properties of the bulk ceramics produced by this precursor route were studied in detail by Riedel et al.[82,83]

Krüger et al.^[19,84] and Smokovych et al.^[33,80,85] studied the oxidation behavior of perhydropolysilazane (PHPS)-based coatings on Mo–Si–B alloys that were obtained by dip coating (see **Figure 27**). The dip coating process has several advantages, for example, short processing time and high flexibility. Furthermore, coating thicknesses with several hundred micrometers can be obtained by repeating the process multiple times. The use of preceramic polymers allows to obtain ceramic coatings while processing at low temperature.^[86] Advantages and disadvantages of the dip coating process are summarized in Figure 27.

However, the polymer-to-ceramic conversion goes along with an inherent volume shrinkage of the coating and the formation of cracks and pores. The shrinkage can exceed more than 50 vol% depending on the polymeric precursor. [87] This is a major disadvantage of this coating strategy, as it is impossible to obtain dense microstructures. Porosity and crack formation, however, can be overcome by adding active or passive particulate fillers to the coating slurry. [88]

Passive fillers do not react with the residues of the ceramic precursor, its gaseous degradation products, or the pyrolysis gas atmosphere. Typically, chemically inert ceramic particles, such Al_2O_3 , ZrO_2 , and SiC, are used as passive fillers. They reduce the volume fraction of the polymeric precursor and fill up voids within the in situ formed PDC. Moreover, they prevent the formation of defects, as they provide opportunities for a release of gaseous products that have formed during pyrolysis (e.g., N_2 , NH_3 , CH_4 , and O_2). [86,89,90]

Active fillers are usually based on metals, intermetallics, carbon, or reactive ceramics, such as Si, B, MoSi₂, or AlN. They fully or partially compensate the shrinkage of the PDC precursor during the polymer-to-ceramic conversion by expansion

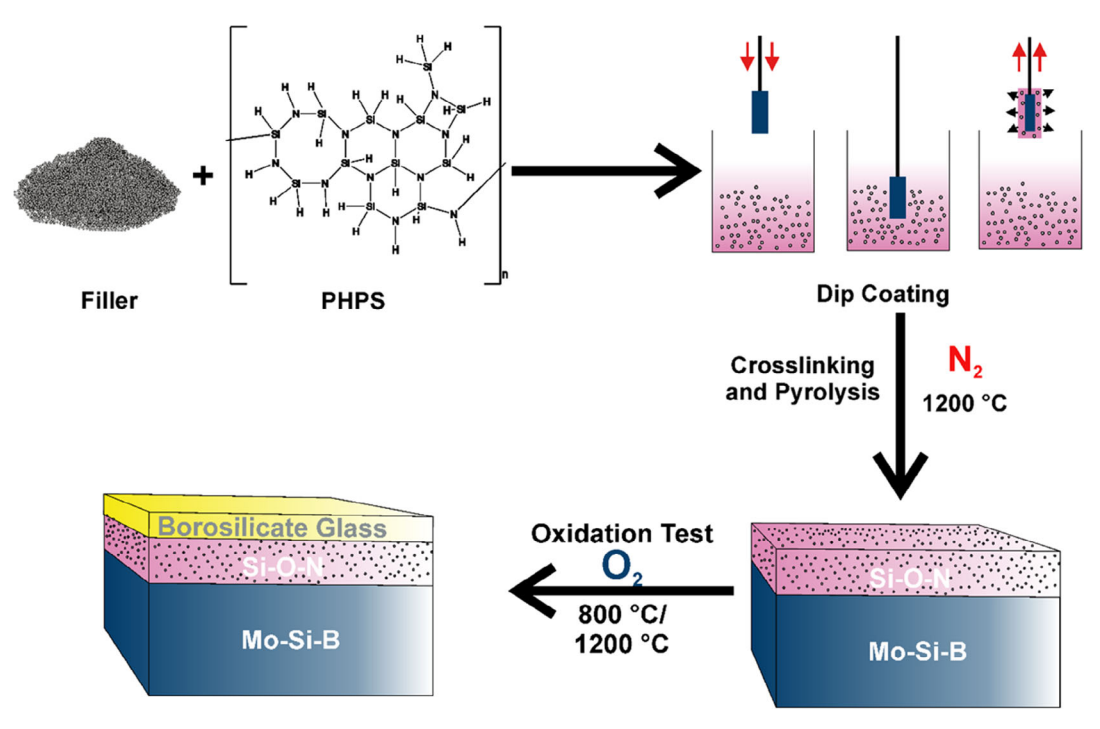


Figure 27. Schematic representation of the dip coating process and PDC consolidation on Mo-Si-B alloys with PHPS precursor.

15272648, 2021, 4, Downloaded from https://onlinelibrary.wiley.com/doi/10.1002/adem.202001016 by Forschungszentrum Jülich GmbH Research Center, Wiley Online Library on [01/05/2024]. See the Terms and Conditions

onditions) on Wiley Online Library for rules of use; OA articles are governed by the applicable Creative Commons

due to reactions of the filler particles with their environment and the formation of new phases. Oxides, nitrides, and carbides can be formed during heat treatment, depending on the polymeric residues, the degassing species, and the pyrolysis atmosphere. [86] Active fillers serve to provide a stabilizing network of filler reaction products, to increase the ceramic yield, and to provide an inner surface, which is required for material transport during polymer decomposition. [89] The microstructural changes during the polymer-to-ceramic conversion with and without fillers are visualized in **Figure 28**.

Schwartz and Rowcliffe^[90] demonstrated that a polymer to filler (Si_3N_4) ratio of 30 wt% yielded the maximum densities for polysilazane-based PDCs. Some of the active fillers are replaced by passive fillers in advanced slurry systems. The passive fillers act as binders and are used to ensure homogeneous mixing of the slurry by minimizing sedimentation effects.^[87]

In addition, fillers can also influence the physical and chemical properties of the coating. [80] However, influencing the chemical composition and reactivity of the coating, fillers can also be used to influence the mechanical properties of the coating. For example, the hardness and elastic modules can be influenced by the filler particles and the formed phases. The CTE of pyrolyzed PHPS is around 3–4 \times 10 $^{-6}$ K $^{-1}$,[86,88,91] and this matches well with the CTE of Mo–Si–B (5.0–6.0 \times 10 $^{-6}$ K $^{-1[28]}$). The CTE mismatch can be further minimized using suitable filler particles, according to the rule of mixture, [92] and thus, stresses resulting from thermal cycling can be reduced.

Smokovych et al. showed the potential to increase the cyclic oxidation resistance of Si–O–N ceramic coatings using active fillers, such as Si, B, SiB₆, and Mo₅SiB₂, which promote the formation of a dense borosilicate-glass scale at the surface during oxidation (see Figure 27). Mo–14Hf–23B and Mo–14.8Zr–26B alloys were coated with PHPS with 24 vol% Si and 12 vol% B via dip coating. Cyclic oxidation tests at 800 °C showed a

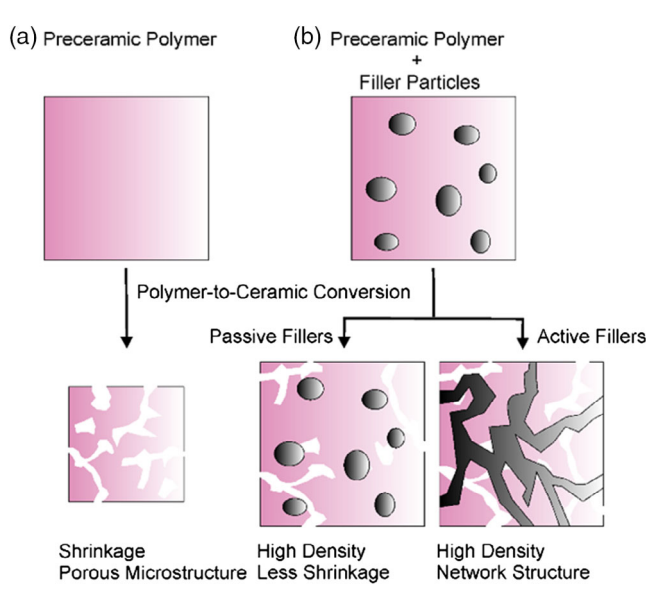


Figure 28. Schematic representation of the evolution of microstructures during polymer-to-ceramic conversion of a) preceramic polymers and b) preceramic polymers with the addition of fillers (adapted from the previous studies^[86,87]).

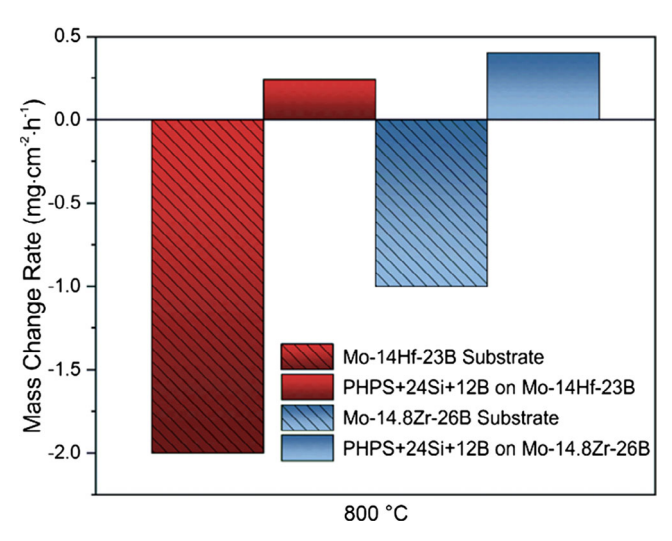


Figure 29. Oxidation behavior of uncoated and with filler-loaded PHPS dip-coated Mo–14Hf–23B and Mo–14.8Zr–26B samples after exposure to air at 800 °C (data from the previous study^[93]).

catastrophic weight loss of the uncoated samples within the first $10\,\mathrm{h}$ of the test, whereas only a small weight increase was observed for the coated samples within $100\,\mathrm{h}$. The high oxidation resistance and the slight weight gain were attributed to the formation of a continuous and dense borosilicate-glass scale on the coatings surface, which further slows down the oxidation kinetics of the samples, leading to stable weight changes for more than $100\,\mathrm{h}$ at $800\,$ and $1100\,^\circ\mathrm{C}$. The test results are visualized in Figure $29.^{[33,80,84,93]}$

Summary Ceramic Coatings: Ceramic coatings are often used in the TBC/EBC field to protect components from corrosion, oxidation, and high temperatures. Compared with metals, ceramic materials offer higher melting temperatures and lower thermal conductivity. However, ceramic coatings are often not fully dense, and the usual adhesion mechanism is mechanical interlocking, which requires proper surface preparation. Ceramic coatings can be obtained by direct coating processes, such as spraying, [45] or by applying ceramic precursors, [33,80,85] e.g., by dip coating and subsequent heat treatment. Coatings with several hundred micrometers can be produced by both methods. Oxidation tests for 1000 h at 1200 °C revealed that dense coatings have a significant higher oxidation resistance. [45] High coating densities of the PDC coatings could be achieved by adding (active) filler particles.^[94] The addition of boron has proved to be particularly promising, as it promotes the formation of an additional, glass-like protective scale. [93]

3. Discussion

Mo and Mo-based alloys suffer from severe pesting at temperatures above $700\,^{\circ}\text{C}$. Alloying with Si and B might increase their oxidation resistance, but the oxidation of Mo, in particular the oxidation of the Mo solid-solution phase, and subsequent evaporation of Mo oxides is still an issue, especially in the temperature range between 800 and $1000\,^{\circ}\text{C}$. There is a variety of different coating techniques, which can be used to produce

com/doi/10.1002/adem.202001016 by Forschun

szentrum Jülich GmbH Research Center, Wiley Online Library on [01/05/2024]. See the Terms and Conditions

on Wiley Online Library for rules of use; OA articles are governed by the applicable Creative Commons

oxidation-resistant coatings for Mo-based alloys. The main coating concept is the application of metallic coatings (mainly MoSi₂), which can form protective oxide scales (mainly silica) in an oxidative atmosphere. The life-determining factor of the $MoSi_2$ coatings is the depletion of Si due to the formation of the Mo_5Si_3 phase, which is susceptible to catastrophic oxidation. $^{[7,76,95]}$

Other coating concepts focus on the direct application of ceramic coatings, which also act as TBC. In particular, the direct application of SiO_2 coatings by spray deposition was studied. A disadvantage is that sprayed ceramic coatings are not completely gas tight, so that the penetration of oxygen cannot be totally avoided. The application of PDCs with active (metallic/metalloid) fillers seems to combine both coating concepts, because they form dense borosilicate-glass scales during high-temperature exposure to air. [33]

The characteristics of the different processes are summarized in **Figure 30** and **Table 2**. The molten salt technique, surface passivation by pre-oxidation, and the CVD process require high process temperatures and long process times. Sputter coating allows for lower temperatures, but due to the low deposition rate (see Figure 30b), only thin coatings can be achieved, even with long coating process durations. Thus, these coating processes are time-consuming, expensive, and may be hard to realize on industrial scale. Other coating techniques, such as dip coating, PTA, and spray techniques, are more versatile: they offer higher deposition rates and are capable of coating large and complex-shaped components more easily.

More relevant than a comparison of the process conditions is a comparative analysis of the protective effect of the different coating concepts. This is quite difficult, because the different approaches were proved using various test conditions (temperature, duration, and cyclic/static) and different coating properties (e.g., thickness and porosity) (see Table S3, Supporting Information). In some coating concepts (e.g., metallic coatings and PDCs), surface oxidation and the associated weight increase through the formation of a protective scale are highly desired. Furthermore, it should be noted that

Table 2. Schematic summary of the characteristics of the coating processes (+ advantageous, - disadvantageous).

Coating method	Process costs	Process duration	Long time protection	Temperature	Technological complexity
Surface passivation	+++	+++			+++
CVD			+++		
Molten salt	+	++	_		+
Liquid siliconizing		+	+		++
Sputter deposition			_	++	
APS	++	+++	++	+	++
Slurry spraying	+++	+++		+++	+++
HVOF	++	+++	+++	++	++
VPS	+	+	+++	+	-
PTA	++	+++	++	+	+
Dip coating	+	++	++	++	++

evaporation of Mo oxides and oxidation of the coating are competing effects, which can occur simultaneously and cannot be considered separately in weight analysis. It is, therefore, possible that the weight losses due to evaporation of Mo oxides and the weight increase due to oxidation of the coating compensate each other and, thus, lead to supposedly low weight change rates. Therefore, it is important to understand the measured values in the context of their system. If a surface oxidation is expected, a significant increase in weight should be observed. The measured weight changes are, therefore, not to be considered as absolute values; they only give an indication of the extent of the oxidation reactions, and whether the evaporation of Mo oxides or the oxidation of other elements is predominant. In general, this applies to all coating processes; a weight loss is critical, as it indicates a (massive) volatilization of Mo oxides.

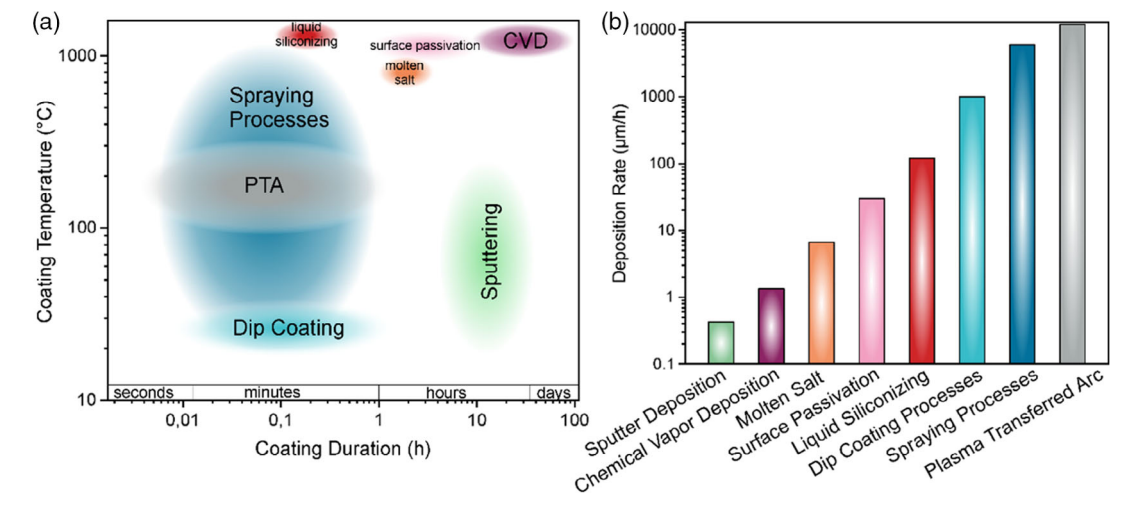


Figure 30. Summarized process characteristics of coating techniques. a) Overview on coating temperature and process duration. b) Overview of the deposition efficiency of different coating processes (data from the previous studies^[28,31,32,38,46,74,101–105])

on Wiley Online Library for rules of use; OA articles are governed by the applicable Creative Commons

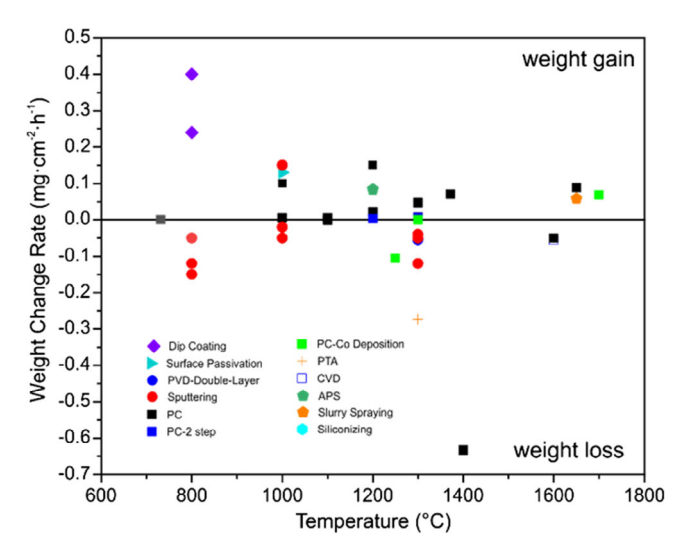


Figure 31. Results of oxidation tests of relevant coating systems (data from the previous studies[28-30,34,37,38,41,56-58,60-62,72,93])

Nevertheless, the results of the oxidation tests of the different coating systems are summarized in Figure 31. To reduce the influence of the different test conditions, a rate was calculated from the measured weight change and plotted against the test temperature. A comparison of the weight changes of coated samples with those of the pure substrates (Figure 4) makes it more clear that all coating systems illustrated have a significant impact on the oxidation behavior of the system.

However, with exception of the PDC dip coating process, all concepts shown are based on metallic coatings, whose key concept is surface oxidation and the formation of a protective oxide scale. Also, in the case of the PCD dip coating concept, the key mechanism is the additional formation of a protective borosilicate-glass scale on top of the ceramic coating. Therefore, a weight gain should be observed in each of these EBC systems. In some systems, however, a weight loss, especially in the critical temperature range between 700 °C and 1000 °C, is still present. This indicates that the oxidation and evaporation of Mo are still major factors in these systems. In this temperature regime, only the dip coating concept shows reasonable weight change rates. As already discussed in the introduction, higher temperatures lead to increased oxidation resistance of Mo-Si-B alloys due to the complex oxidation mechanism. Therefore, above 1200 °C, the weight change rates of coatings produced by spraying or PC become more reasonable.

Yet, these values are still difficult to compare, especially because the oxidation kinetics can change throughout the test. It is, therefore, essential to understand the oxidation behavior of the substrate and the coating material and to consider them separately to evaluate the protective effect of the coating. For example, Krüger et al.[84] and Smokovych et al.[80] recently published detailed studies on the oxidation behavior of free-standing PDC coatings. Comparative studies with freestanding coatings, substrates, and substrate coating systems might help to evaluate the oxidation behavior and the protection efficiency of the coating systems. A detailed study on the oxidation behavior of Mo-9Si-8B was published by Azim et al. [96] The group successfully developed a model to separate the measured weight gain and loss effects and, thus, calculate the actual material damage of this alloy.

Another factor that would help to evaluate the different coating concepts is the lifetime analysis of coated samples that have been tested under realistic conditions. Tang et al. [57] published predicted lifetimes of Si-PC coatings. The reaction rate from MoSi₂ to Mo₅Si₃ was used as basis for this calculation. At 1100 °C, a lifetime of 20 000-300 000 h (2-34 years) was predicted for this specific coating system. The calculated maximum lifetime decreases drastically with increasing temperature. The exponential decrease in the expected maximum lifetime is shown in Figure 32. However, there are currently no studies that can confirm or disprove these lifetimes for this or any other coating system. Therefore, in addition to the fundamental investigation of the oxidation behavior of the coating and substrate, more lifetime studies should be carried out. This includes a thorough analysis of the coating adhesion (cycle to failure, pull adhesion tests), especially of the ceramic coatings. As the metallic coatings are bonded to the substrate by diffusion bonding, [29] the adhesion strength of these coatings should be relatively high; however, under thermo-cyclic conditions, cracks may form in the coating or in the oxide scale, which could lead to spallation or chipping.

4. Conclusion

Mo-based alloys, among them Mo-Si-B alloys, are promising candidates for high-temperature turbine applications; however, they suffer from massive oxidation and volatilization of Mo in the temperature range from 700 to 1000 °C. Therefore, additional oxidation protection is necessary for using the material in hightemperature processes in air. In this article, the state of the art of research on oxidation protection coatings for Mo-based alloys was presented.

It was found that coating systems containing metallic Si and B can form protective borosilicate-glass scales to limit oxygen diffusion. Both can be provided by a variety of coating processes

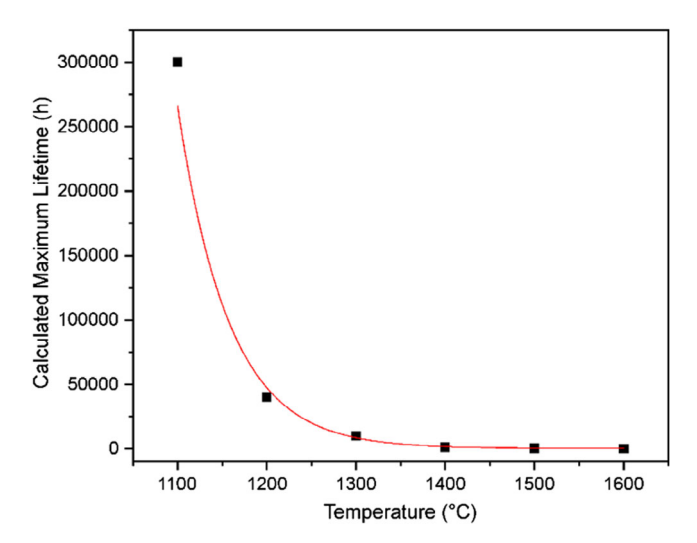


Figure 32. Calculated maximum coating lifetime at different temperatures (data from the previous study, [57] red line: guideline to the eye).

15272648, 2021, 4, Downloaded from https://onlinelibrary.wiley.com/doi/10.1002/adem.202001016 by Forschungszentrum Jülich GmbH Research Center, Wiley Online Library on [01/05/2024]. See the Terms and Conditions

conditions) on Wiley Online Library for rules of use; OA articles are governed by the applicable Creative Commons



with different performance resulting from processing parameters, such as processing time to achieve the desired coating, processing temperature and pressure, starting materials, and, last but not least, the complexity of the processing equipment and the total costs of the coating process. These parameters must be optimized and directly influence the economic and protection efficiency of the process and the coating, respectively.

Another concept is the use of ceramic SiO₂ coatings, which, however, do not provide long-term protection of the substrate, because they are not gas tight. A combination of both concepts-Si and B embedded in a silica or ceramic matrix—is promising due to an extremely low oxidation rate.

Therefore, we propose that the following holds: 1) Research should focus on the combination of active fillers (for glass formation) in a ceramic matrix; this also holds the potential for tailored adhesion and CTE mismatch between substrate and coating, 2) to gain deeper insight into the sub-processes of oxidation and glass formation, more effort should be spent on separate investigations of the coating material and the substrate material, and 3) life-cycle analysis of tests carried out under realistic conditions as well as life-time simulations of the protective function of coatings may be the key to a successful coating development strategy; this is independent of the coating process and can provide scope for transfer to other refractory metal alloys.

Supporting Information

Supporting Information is available from the Wiley Online Library or from the author.

Acknowledgements

The authors gratefully acknowledge the Deutsche Forschungsgemeinschaft (DFG) for financial support (Grant No. 317275772).

Conflict of Interest

The authors declare no conflict of interest.

Keywords

environmental barrier coatings, Mo-based alloys, Mo-Si-B alloys, oxidation protection

> Received: August 28, 2020 Revised: November 28, 2020 Published online: December 18, 2020

- [1] J. H. Perepezko, Science 2009, 326, 1068.
- [2] A. Vardelle, C. Moreau, J. Akedo, H. Ashrafizadeh, C. C. Berndt,
 - J. O. Berghaus, M. Boulos, J. Brogan, A. C. Bourtsalas,
 - A. Dolatabadi, M. Dorfman, T. J. Eden, P. Fauchais, G. Fisher,
 - F. Gaertner, M. Gindrat, R. Henne, M. Hyland, E. Irissou,
 - E. H. Jordan, K. A. Khor, A. Killinger, Y.-C. Lau, C.-J. Li, L. Li,
 - J. Longtin, N. Markocsan, P. J. Masset, J. Matejicek, G. Mauer, et al., J. Thermal Spray Technol. 2016, 25, 1376.

- [3] J. A. Lemberg, R. O. Ritchie, Adv. Mater. 2012, 24, 3445.
- [4] R. L. Fleischer, JOM 1985, 37, 16.
- [5] T. Geng, C. Li, X. Zhao, H. Xu, Z. Du, C. Guo, Calphad 2010, 34, 363.
- [6] R. F. de Farias, C. Airoldi, J. Phys. Chem. Solids 2003, 64, 2199.
- [7] J. H. Schneibel, J. A. Sekhar, Mater. Sci. Eng. A 2003, 340, 204.
- [8] M. K. Meyer, A. J. Thom, M. Akinc, Intermetallics 1999, 7, 153.
- [9] T. A. Parthasarathy, M. G. Mendiratta, D. M. Dimiduk, Acta Mater. **2002**, 50, 1857.
- [10] R. H. Lamoreaux, D. L. Hildenbrand, L. Brewer, J. Phys. Chem. Ref. Data 1987, 16, 421.
- [11] T. Karahan, G. Ouyang, P. K. Ray, M. J. Kramer, M. Akinc, Intermetallics 2017, 87, 38.
- [12] M. F. Yan, J. B. Macchesney, S. R. Nagel, W. W. Rhodes, J. Mater. Sci. **1980**, 15, 1371.
- [13] J. E. Gardner, M. Hilton, M. R. Carroll, Geochim. Cosmochim. Acta 2000, 64, 1473.
- [14] F. A. Rioult, S. D. Imhoff, R. Sakidja, J. H. Perepezko, Acta Mater. **2009**, 57, 4600.
- [15] M. G. Mendiratta, T. A. Parthasarathy, D. M. Dimiduk, Intermetallics 2002, 10, 225.
- [16] S. Burk, B. Gorr, M. Krüger, M. Heilmaier, H. J. Christ, JOM 2011, 63, 32.
- [17] J. A. Lemberg, M. R. Middlemas, T. Weingärtner, B. Gludovatz, J. K. Cochran, R. O. Ritchie, Intermetallics 2012, 20, 141.
- [18] G. Hasemann, D. Kaplunenko, I. Bogomol, M. Krüger, JOM 2016, 68, 2847-2853.
- [19] M. Krüger, G. Hasemann, T. Baumann, S. Dieck, S. Rannabauer, MRS Proc. 2015, 1760, https://doi.org/10.1557/opl.2015.28.
- [20] M. Krüger, P. Jain, K. S. Kumar, M. Heilmaier, Intermetallics 2014, 48, 10.
- [21] M. Krüger, S. Franz, H. Saage, M. Heilmaier, J. H. Schneibel, P. Jéhanno, M. Böning, H. Kestler, Intermetallics 2008, 16, 933.
- [22] H. B. Guo, R. Vaßen, D. Stöver, Surface Coat. Technol. 2004, 186, 353.
- [23] X. Wang, P. Xiao, Acta Mater. 2004, 52, 2591.
- [24] A. M. Limarga, R. Vaßen, D. R. Clarke, J. Appl. Mech. 2011, 78.
- [25] C. Li, X. Zhang, Y. Chen, J. Carr, S. Jacques, J. Behnsen, M. di Michiel, P. Xiao, R. Cernik, Acta Mater. 2017, 132, 1.
- [26] R. K. Sharmaa, A. K. Upadhyay, S. B. Sharma, Int. J. Eng. Technol. Sci. Res. 2017, 4, 464.
- [27] D. Tejero-Martin, C. Bennett, T. Hussain, J. Eur. Ceram. Soc. 2020.
- [28] A. Lange, R. Braun, M. Heilmaier, Intermetallics 2014, 48, 19.
- [29] X. Deng, G. Zhang, T. Wang, S. Ren, Y. Shi, Z. Bai, Q. Cao, Ceramics Int. 2019, 45, 415-423.
- [30] A. Lange, R. Braun, U. Schulz, Mater. High Temp. 2018, 35, 195.
- [31] R. O. Suzuki, M. Ishikawa, K. Ono, J. Alloys Compd. 2000, 306,
- [32] Y. Zhang, Y. Li, C. Bai, Ceram. Int. 2017, 43, 6250-6256.
- [33] I. Smokovych, G. Hasemann, M. Krüger, M. Scheffler, J. Eur. Ceram. Soc. 2017, 37, 4559.
- [34] J. H. Perepezko, Int. J. Refract. Metal Hard Mater. 2018, 71, 246.
- [35] J.-K. Yoon, J.-K. Lee, J.-Y. Byun, G.-H. Kim, Y.-H. Paik, J.-S. Kim, Surf. Coat. Technol. 2002, 160, 29.
- [36] A. R. Cox, R. Brown, J. Less Common Metals 1964, 6, 51.
- [37] S. P. Chakraborty, S. Banerjee, I. G. Sharma, A. K. Suri, J. Nucl. Mater. 2010, 403, 152.
- [38] K. Choi, W. Yang, K.-H. Baik, Y. Kim, S. Lee, S. Lee, J. S. Park, Appl. Surf. Sci. 2019, 489, 668.
- [39] J. S. Park, J. M. Kim, H. Y. Kim, S. Yi, J. H. Perepezko, Metals Mater. Int. 2008, 14, 1.
- [40] M. Z. Alam, B. Venkataraman, B. Sarma, D. K. Das, J. Alloys Compd. 2009. 487. 335.
- [41] Z. Cai, S. Liu, L. Xiao, Z. Fang, W. Li, B. Zhang, Surface Coat. Technol. **2017**, 324, 182.

on Wiley Online Library for rules of use; OA articles are governed by the applicable Creative Commons

1005-1009.

www.advancedsciencenews.com

ENGINEERING

www.aem-journal.com

- [78] G. Mera, E. Ionescu, in Encyclopedia of Polymer Science and
- [43] J.-H. Yan, X. Jian-jian, d. Rafi ud, Y. Wang, L.-F. Liu, Ceram. Int. 2015, 41, 10547.

[42] P. Jéhanno, M. Heilmaier, H. Kestler, Intermetallics 2004, 12,

- [44] G. Reisel, B. Wielage, S. Steinhäuser, I. Morgenthal, R. Scholl, Surf.
- Coat. Technol. 2001, 146-147, 19. [45] J. H. Perepezko, F. Rioult, R. Sakidja, Mater. Sci. Forum 2008,
- 595-598, 1065. [46] V. Behrani, A. J. Thom, M. J. Kramer, M. Akinc, Metall. Mater. Trans. A 2005. 36. 609.
- [47] T. Hsieh, H. Choe, E. J. Lavernia, J. Wolfenstine, Mater. Lett. 1997, 30, 407
- [48] H. Zhang, J. Lv, Y. Wu, S. Gu, Y. Huang, Y. Chen, Ceram. Int. 2015, 41, 14890
- [49] H. Zhang, S. Gu, Int. J. Refract. Metal Hard Mater. 2013, 41, 128.
- [50] R. Bianco, R. A. Rapp, in Metallurgical and Ceramic Protective Coatings (Ed.: K. H. Stern), Springer Netherlands, Dordrecht 1996, pp. 236.
- [51] J. H. Perepezko, R. Sakidja, JOM 2010, 62, 13.
- [52] J.-Y. Byun, J.-K. Yoon, G.-H. Kim, J.-S. Kim, C.-S. Choi, Scr. Mater. **2002**, 46, 537.
- [53] J. Sun, Q.-G. Fu, L.-P. Guo, Y. Liu, C.-X. Huo, H.-J. Li, Mater. Design 2016, 92, 602.
- [54] S. Majumdar, Surf. Coat. Technol. 2012, 206, 3393.
- [55] P. Zhang, X. Guo, C. Zhang, Q. Tao, C. Shen, Int. J. Refract. Metal Hard Mater. 2017, 67, 32.
- [56] R. Sakidja, F. Rioult, J. Werner, J. H. Perepezko, Scripta Mater. 2006, 55, 903.
- [57] Z. Tang, A. J. Thom, M. J. Kramer, M. Akinc, Intermetallics 2008, 16, 1125.
- [58] A. Lange, M. Heilmaier, T. A. Sossamann, J. H. Perepezko, Surf. Coat. Technol. 2015, 266, 57.
- [59] J. H. Perepezko, MRS Adv. 2017, 2, 1323.
- [60] X. Tian, X. Guo, Z. Sun, Z. Yin, L. Wang, Int. J. Refract. Metal Hard Mater. 2014, 45, 8.
- [61] Y. Wang, D. Wang, J. Yan, J. Alloys Compd. 2014, 589, 384.
- [62] Y. Wang, J. Yan, D. Wang, Int. J. Refract. Metal. Hard Mater. 2017, 68, 60,
- [63] S. Kim, J. H. Perepezko, J. Phase Equil. Diffus. 2006, 27, 605-613.
- [64] I. P. Downs, J. H. Perepezko, R. Sakidja, S. R. Choi, Surf. Coat. Technol. 2014, 239, 138.
- [65] A. Y. C. Nee, Handbook of Manufacturing Engineering and Technology, Springer-Verlag-London, London, 2015.
- [66] O. Auciello, J. Engemann, Multicomponent and Multilayered Thin Films for Advanced Microtechnologies: Techniques, Fundamentals and Devices, 1993
- [67] S. Govindarajan, B. Mishra, D. L. Olson, J. J. Moore, J. Disam, Surf. Coat. Technol. 1995, 76-77, 7.
- [68] R. Vaßen, E. Bakan, C. Gatzen, S. Kim, D. Mack, O. Guillon, Coatings **2019** 9 784
- [69] A. Kotousov, S.-Y. Ho, P. Nguyen, Surf. Innovat. 2013, 1, 190.
- [70] P. L. Fauchais, J. V. R. Heberlein, M. I. Boulos, Thermal Spray Fundamentals, Springer, New York, 2014.
- [71] X. Fei, Y. Niu, H. Ji, L. Huang, X. Zheng, Ceram. Int. 2011, 37, 813.
- [72] Y. Wang, D. Wang, J. Yan, A. Sun, Appl. Surf. Sci. 2013, 284, 881.
- [73] N. Nomura, T. Suzuki, K. Yoshimi, S. Hanada, Intermetallics 2003, 11, 735.
- [74] Gemeinschaft Thermisches Spritzen e.V., Was ist Thermisches Spritzen? https://www.gts-ev.de/html_d/ts-info.htm#v_PTA, (accessed: April 2020).
- [75] M. K. Meyer, Retrospective Theses and Dissertations 1995, https://lib.dr. iastate.edu/rtd/10935.
- [76] M. K. Meyer, M. Akinc, J. Am. Ceram. Soc. 1996, 79, 938.
- [77] M. Günthner, T. Kraus, W. Krenkel, G. Motz, A. Dierdorf, D. Decker, Int. J. Appl. Ceram. Technol. 2009, 6, 373.

- Technology 2013.
- [79] O. Goerke, E. Feike, T. Heine, A. Trampert, H. Schubert, J. Eur. Ceram. Soc. 2004, 24, 2141.
- [80] I. Smokovych, M. Krüger, M. Scheffler, J. Eur. Ceram. Soc. 2019, 39, 3634.
- [81] R. Riedel, G. Passing, H. Schönfelder, R. J. Brook, Nature 1992, 355, 714.
- [82] R. Riedel, H.-J. Kleebe, H. Schönfelder, F. Aldinger, Nature 1995, 374, 526.
- [83] R. Riedel, G. Mera, R. Hauser, A. Klonczynski, J. Ceram. Soc. Jpn. 2006, 114, 425.
- [84] M. Krüger, J. Schmelzer, I. Smokovych, J. Lopez Barrilao, G. Hasemann, Powder Technol. 2019, 352, 381.
- [85] I. Smokovych, M. Scheffler, Adv. Eng. Mater. 2018, 20.
- [86] P. Colombo, G. Mera, R. Riedel, G. D. Sorarù, J. Am. Ceram. Soc. 2010, 93, 1805.
- [87] P. Greil, J. Am. Ceram. Soc. 1995, 78, 835.
- [88] M. Günthner, A. Schütz, U. Glatzel, K. Wang, R. K. Bordia, O. Greißl, W. Krenkel, G. Motz, J. Eur. Ceram. Soc. 2011, 31, 3003.
- [89] I. Petríková, M. Parchovianský, P. Švančárek, M. Lenz Leite, G. Motz, D. Galusek, Int. J. Appl. Ceram. Technol. 2020, 17, 998.
- [90] K. B. Schwartz, D. J. Rowcliffe, J. Am. Ceram. Soc. 1986, 69, C-106.
- [91] I. Smokovych, C. Gatzen, M. Krüger, M. Scheffler, Materials 2020, 13, 4878.
- [92] H. A. Bruck, B. H. Rabin, J. Am. Ceram. Soc. 1999, 82, 2927.
- [93] I. Smokovych, V. Bolbut, M. Krüger, M. Scheffler, Materials 2019, 12,
- [94] I. Smokovich, C. Gatzen, M. Krüger, M. Schwidder, M. Scheffler, Materials 2020, 13.
- [95] M. Akinc, M. K. Meyer, M. J. Kramer, A. J. Thom, J. J. Huebsch, B. Cook, Mater. Sci. Eng. A 1999, 261, 16.
- [96] M. A. Azim, B. Gorr, H. J. Christ, M. Heilmaier, U. Koch, M. Engelhard, Oxid. Metal. 2017, 87, 89.
- [97] Matt Hughes President Semicore Equipment Inc., What Is Sputtering? Magnetron Sputtering?, http://www.semicore.com/ what-is-sputtering, (accessed: March 2020).
- [98] O. Metco, Thermal Spray Brochure 2016, 6.
- [99] F. S. Technologies, Thermal Spray Technology, Information Brochue, 2016.
- [100] Durum Verschleißschutz GmbH, Hard-facing Plasma-Transferred-Arc Welding (PTA), https://durmat.com/en/service/hard-facing/, (access: March 2020).
- [101] S. R. Choi, N. P. Bansal, D. Zhu, Mechanical and Thermal Properties of Advanced Oxide Materials for Higher-Temperature Coatings Applications, NASA Report, 2004.
- [102] S. Rajendran, T. A. Nguyen, S. Kakooei, M. Yeganeh, Y. Li, Corrosion Protection at the Nanoscale -1st Edition, Elsevier, Amsterdam 2020.
- [103] A. Baptista, F. Silva, J. Porteiro, J. Míguez, G. Pinto, Coatings 2018, 8.
- [104] A. Mohammadzadeh, S. K. Naghib Zadeh, M. H. Saidi, M. Sharifzadeh, in Design and Operation of Solid Oxide Fuel Cells (Ed.: M. Sharifzadeh), Academic Press, Cambridge, MA 2020, pp. 85-130.
- [105] A. Torabi, T. H. Etsell, P. Sarkar, Solid State Ion. 2011, 192, 372.
- [106] P. Hidnert, H. S. Krider, J. Res. Natl Bur. Stand. 1952, 48, 209.
- [107] J. Franklin Inst. 1930, 210, 104.
- [108] E. Weintraub, J. Industr. Eng. Chem. 1913, 5, 106.
- [109] S. N. Achary, S. J. Patwe, M. D. Mathews, A. K. Tyagi, J. Phys. Chem. Solids 2006, 67, 774.
- [110] N. P. Bansal, S. R. Choi, Ceram. Int. 2015, 41, 3901.
- [111] Plansee S. E., Chromium, https://www.plansee.com/en/materials/ chromium.html, (accessed: May 2020).
- [112] G. C. A. M. Janssen, F. D. Tichelaar, C. C. G. Visser, J. Appl. Phys. **2006**, 100, 0935121.

ADVANCED ENGINEERING

www.advancedsciencenews.com www.aem-journal.com

- [113] B. S. Rabinovich, I. Z. Radovskii, P. V. Gel'd, Sov. Powder Metall. Metal Ceram. 1968, 7, 879.
- [114] E. I. Zoz, E. N. Fomichev, A. A. Kalashnik, G. G. Eliseeva, Russ. J. Inorg. Chem. 1982, 27, 54–56.
- [115] P. Hindert, W. B. Gero, Sci. Papers Bur. Stand-488 1924, 19, 429.
- [116] W. Martienssen, H. Warlimont, Springer Handbook of Condensed Matter and Materials Data, Springer, Berlin, Heidelberg, 2005.
- [117] D. L. Perry, S. L. Phillips, Handbook of Inorganic Compounds, CRC Press, Boca Raton 1995.
- [118] H. L. Zhao, M. J. Kramer, M. Akinc, Intermetallics 2004, 12, 493.
- [119] T. Middelmann, A. Walkov, G. Bartl, R. Schödel, *Phys. Rev. B* **2015**, 92, 174113.

- [120] R. S. Feigelson, W. D. Kingery, Ceram. Bull. 1963, 42, 688.
- [121] K. N. Lee, R. A. Miller, N. S. Jacobson, J. Am. Ceram. Soc. 1995, 78, 705.
- [122] T. Okamoto, Y. Ukyo, J. Mater. Sci. 1997, 32, 2473.
- [123] L. Neckel Jr, A. G. Weiss, G. Motz, D. Hotza, M. C. Fredel, Adv. Mater. Res. 2014, 975, 149.
- [124] P. Hidnert, J. Res. Natl. Bur. Stand. 1943, 30, 101-105.
- [125] M. S. Ahmed, X. Zhao, Z.-F. Zhou, P. Munroe, N. Chen-Tan, L. K. Y. Li, Z. Xie, J. Am. Ceram. Soc. 2011, 94, 1546-1551.
- [126] P. Hidnert, W. T. Sweeney, Sci. Papers Bur. Stand. 1925, 20, 483.
- [127] M. Fritsch, H. Klemm, Fraunhofer Gesellschaft.



Caren Gatzen has studied Chemistry at the RWTH Aachen University, focusing on catalysis and solid-state chemistry, especially on ceramics. After obtaining her M.Sc. degree in 2015, she began her doctorate at Forschungszentrum Jülich, intensely working on thermally sprayed EBCs for ceramics matrix composites. Since 2019, she has been working as a Research Associate in a project of Otto von Guericke University Magdeburg and Forschungszentrum Jülich GmbH, where she has been investigating preceramic polymer-based EBCs for refractory metals.



Iryna Smokovych has been working on the development of new materials and heat treatment processes for steel, aluminum, and titanium alloys, since 2004. She completed her studies in this field in 2015 with a Ph.D. thesis at the National Technical University of Ukraine "Kyiv Polytechnic Institute NTUU "KPI." During her doctoral thesis, she worked on diffusion-inhibiting coatings for titanium alloys. Later, she was involved in the project of the preceramic polymers application as oxidation protective coatings of Otto von Guericke University Magdeburg. Since 2015, she has been a Research Associate with the Institute of Materials, Chair of Nonmetallic and Composite Materials.



Michael Scheffler received a Ph.D. from Martin-Luther University, Halle, Germany, in 1993. From 1994 to 1998 he was senior scientist with the Institute for Physical High-Technology, Jena, Germany, afterwards he started his work with the university of Erlangen-Nuremberg. In 2003 he was granted a scholarship from DFG for a stay at the university of Washington in Seattle. Afterwards he became head of division of the Center for Advanced Energy Research in Erlangen. In 2006, he moved to Brandenburg Technical University and established a professorship for light weight ceramics. In 2009 he moved to Otto-von-Guericke University in Magdeburg as a professor for materials technology of nonmetallic materials and composites. His research deals with PDCs and their reactions with particulate fillers, a great variety of aspects of cellular ceramics ranging from basic manufacturing processes over surface modification to heat storage applications, and on coatings for materials protection. Michael Scheffler is member of the Saxon Academy of Sciences and Humanities.



Manja Krüger received her Ph.D. in 2010 in Mechanical Engineering/ Materials Science at Otto-von-Guericke University Magdeburg, where she developed powder metallurgical processes for molybdenum silicide alloys. In 2012 she started working as Assistant Professor for Intermetallic Materials. Since 2017 she was Professor at RWTH Aachen University and at the same time head of the group "Mechanics of Materials" at Forschungszentrum Jülich. Her research activities focused on metals and ceramics for applications in various energy-related systems. In 2019 she became Chair of "High Temperature Materials" at Otto-von-Guericke University Magdeburg, where she develops new materials and compounds, e.g. ingot and powder metallurgically processed metals and multi-principal element alloys, 3D printed aluminides and silicides, and biocompatible materials with and without coatings. Her focus is on the characterization of materials behavior at different length-scales under complex mechanical and thermal loadings.